HIGH TEMPERATURE MECHANICAL CHARACTERISTICS OF FRICTION STIR PROCESSED LIGHT ALLOYS

A Thesis

by

Ali Hosseinzadeh Ghobadlou

Submitted to the

Graduate School of Sciences and Engineering
In Partial Fulfillment of the Requirements for
the Degree of

Master of Science

in the
Department of Mechanical Engineering

Özyeğin University
August 2018

HIGH TEMPERATURE MECHANICAL CHARACTERISTICS OF FRICTION STIR PROCESSED LIGHT ALLOYS

Approved by:

Assoc. Prof. Dr. Güney Güven Yapıcı,
Advisor,
Department of Mechanical Engineering
Özyeğin University

Asst. Prof. Dr. Alpay Oral,
Department of Mechanical Engineering
Yıldız Technical University

Asst. Prof. Dr. Zeynep Başaran Bundur,
Department of Civil Engineering
Özyeğin University

Date Approved: 1 August 2018

DEDICATION

To My Family

ABSTRACT

Friction stir processing (FSP) is a recently developed process for surface modification of light alloys that has expanded into applications other than microstructure refinement by the concept of fabricating metal matrix composites (MMCs). FSP as a severe plastic deformation method also enables the manufacturing of high strength materials.

Although considerable research has been done to observe the microhardness and corrosion resistance of MMCs and FSPed alloys, rather less attention has been paid to the high temperature mechanical properties and fracture mechanisms of aforementioned materials. This study investigates fabrication of aluminum and magnesium MMCs via FSP and tracks the ambient and high temperature mechanical behavior of processed materials. In order to understand the effect of FSP parameters on the tensile behavior, experimental design methods were utilized. The microstructure evolution and distribution of dispersed particles were observed. It was shown that embedding SiC reinforcements improved the microhardness of FSPed samples up to 50% and 80% relative to the as-received Al2024 and AZ31 conditions.

Ambient temperature tensile tests were performed and the results revealed that the yield strength of Al2024 samples improved about 2.5 folds, in relation with the refined microstructure after FSP with the expense of decreasing ductility to about 4%. While FSP decreased the yield strength of AZ31 to 80 MPa along with increasing ductility up to 26%. Therefore, formability of AZ31 sharply increased at room temperature.

High temperature tensile tests were conducted at 300˚C under strain rates of 0.01 s^{-1}, 0.001 s^{-1}, 0.0001 s^{-1} and strain rate sensitivity (m) of both Al2024 and AZ31 were determined

for all conditions. The results exhibited that *m* value of Al2024 increased up to 0.16 for FSPed sample while *m* value of AZ31/SiC MMC was stable at 0.21 for all interval strain levels.

Fracture surface analysis after high temperature loading revealed that the mechanism at high strain rate is dominated by intergranular fracture for fine grained FSPed and MMC samples of Al2024, while the as-received sample is generally fractured by coalescence of microvoids even under high strain rate. On the other hand, the ductile fracture of fine grained FSPed samples represented by equiaxed and relatively deep micro voids were observed for AZ31, whereas the annealed and MMC samples revealed a relatively brittle fracture.

ÖZET

Sürtünme karıştırma işleme, hafif alaşımların yüzey modifikasyonları için kullanılan bir teknik olmakla birlikte uygulama alanı genişleyerek metal matrisli kompozit üretimi için de kullanılmaya başlanmıştır.

Metal matrisli kompozitler ve sürtünme karıştırma işleme yapılmış alaşımların mikrosertlik ve korozyon dayanımlarını gözlemlemeye yönelik kaydedeğer sayıda çalışma yapılmış olmasına rağmen, bu malzemelerin yüksek sıcaklık davranışları ve kırılma mekanizmalarıyla alakalı çalışmalara literatürde oldukça az rastlanmıştır. Bu çalışmada, sürtünme karıştırma işleme ile elde edilen alüminyum ve magnezyum metal matrisli kompozitler ve bunların oda sıcaklığı ve yüksek sıcaklıklardaki mekanik davranışları incelenmiştir. Sürtünme karıştırma işlemi parametrelerinin etkilerini anlamak için deney tasarım metotları kullanılmıştır. Çökelmiş partiküllerin mikroyapı gelişimi ve dağılımı incelenmiştir. SiC takviyeli metal matrisli kompozitlerin mikrosertlik değerlerinin başlangıç durumdaki Al2024 ve AZ31'e göre sırasıyla %50 ve %80 arttığı gözlenmiştir.

Oda sıcaklığındaki çekme testlerinin sonuçlarına göre sürtünme karıştırma işleme sonrası mikroyapı incelmesiyle beraber Al2024 numunelerinin akma dayanımları 2.5 kat artmıştır. Sürtünme karıştırma işleme AZ31 numunelerinin akma dayanımlarını 80 MPa'ya düşürürken sünekliğini %26 artırmıştır, bu sayede AZ31'in oda sıcaklığındaki şekillendirilebilirliği de dikkate değer ölçüde artmıştır.

Yüksek sıcaklıktaki testler 300°C'de ve 0.01 s^{-1}, 0.001 s^{-1}, 0.0001 s^{-1} gerinim hızlarında gerçekleştirilmiştir ve tüm koşullar için Al2024 ve AZ31'in gerinim duyarlılıkları

belirlenmiştir. Sonuçlara göre Al2024'ün m değeri, sürtünme karıştırma işleme sonrası numunelerde 0.16'ya yükselirken; AZ31 numunelerinde tüm gerinim seviyelerinde 0.21 değerinde sabit kalmıştır.

Yüksek sıcaklık yükleme sonrası yapılan kırılma yüzeyi analizi, başlangıç durumdaki Al2024 numunelerin genellikle yüksek gerinim hızında bile mikro boşlukların birleşimiyle kırılırken, yüksek gerinim hızında, sürtünme karıştırma işlemeye tabi tutulmuş ince taneli numuneleri için taneler arası kırılmanın egemen olduğunu ortaya koymuştur. Öte yandan, sürtünme karıştırma işleme sonrası AZ31 numunelerinin eş eksenli ve nispeten derin mikro boşluklu şekilde sünek kırıldığı gözlenirken, başlangıç durum ve metal matrisli kompozit numunelerin nispeten gevrek kırıldığı belirlenmiştir.

ACKNOWLEDGEMENTS

First and foremost, I would like to thank my supervisor, Dr. Güney Güven Yapıcı, for his great guidance and limitless support throughout the course of my research work. I am indebted to him for his continual encouragement and support to carry out the current study.

On the other hand, I would like to thank my MSc. committee members, Asst. Prof. Dr. Alpay Oral and Asst. Prof. Dr. Zeynep Başaran Bundur for their guidance and attention to this study.

I would like to thank our technician of the manufacturing laboratory, Mr. Ulaş Yıldırım, for his contributions in this work and also my colleagues in the MEMFIS group Görkem M. Şimşek, Onur Bilgin and Ibrahim Orhun Tugay for the enjoyable time I have passed with them. Special thanks go to my best friend Salar Salahi who has made a valuable helps and suggestions during my bachelor and master education. I would also like to thank my former colleague, Dr. Seyed Vahid Sajadifar, for his limitless help and valuable comments, it was my honor to work with him at MEMFIS group.

I highly appreciate my beloved family, specially my parents, who dedicated their lives to support me throughout my school and university years and deeply thank my dear sister, Zahra and my brother, Ata for their support and kindness.

Finally, I would like to thank my volleyball teammate, Doğa who provides me the opportunity to meet with lovely friends, Umut, Ali, Burak, Deniz, Gökhan, Ebru, Gizem, Erdem, Ezgi, Ozan and Şebnem. They embraced me in Turkey and I didn’t feel the absence of my family. They will stay in my heart as long as I am living this life.

TABLE OF CONTENTS

LIST OF TABLES

LIST OF FIGURES

1 INTRODUCTION

1.1 Motivation

For many years, researchers have made persistent efforts to enhance mechanical properties of structural materials by using different methods. Alloying a metal with other metals or non-metals was one of the common methods which often improves its strength or even ductility. But the further process still needs to be performed to achieve the satisfactory strength to weight ratio for several structural parts in aerospace and automotive industries.

Fabrication of composites is one of the important processes with the aim of strengthening the alloys. Composites can provide advanced physical, chemical, and mechanical properties for different applications. Composite materials are typically classified by the type of reinforcement they use. This reinforcement is embedded into a matrix that holds it together. The reinforcement is utilized to strengthen the composite. Common composite types include filler reinforcement, random-fiber or short-fiber reinforcement, long-fiber reinforcement, flake reinforcement and particulate reinforcement.

Nowadays, researchers are working on different methods of making metal matrix composites (MMCs) with embedding the micro and nano particles inside of the matrix. General types of these methods of MMC fabrication are liquid state and solid state. Powder metallurgy, ultrasonic assisted casting, diffusion bonding and friction stir processing (FSP) are the most applicable techniques of solid state fabrication methods of MMCs. Friction stir processing (FSP) is a relatively new surface modification technique based on the basic principle of friction stir welding (FSW).

Friction stir welding (FSW) is a solid-state joining method that uses a non-consumable tool to join two workpieces without melting the workpiece material. Heat is generated by friction between the rotating tool and the material, which leads to a softened area near the FSW tool. While the tool is traversed along the joint line, it mechanically intermixes the two parts of metal, and forges the hot and softened metal by the mechanical pressure, applied by the tool.

In addition to surface modification, severe plastic deformation (SPD) during FSP leads to the significant grain refinement. Adding the ceramic particles to the matrix with using FSP in order to have a homogenized MMC is one of the most important advantage of this method. The FSP method is a solid state process thus solidification structure is absent and the problem interrelated to the existence of brittle eutectic and interdendritic phases is eliminated.

Also another advantage of FSP method is the capability of adding the reinforcement particles into the thicker region of the surface and it can be help to improve mechanical properties of metal matrix composites. With considering the previous works and the applications of magnesium and aluminum based MMCs it can be understood that there is a lack of investigation in high temperature tensile behavior at different strain rates of the MMCs manufactured by FSP. Aforementioned lack of data about the mechanical behavior at high temperature limits the application of these composites. Effects of embedding ceramic particles inside of light alloys matrix on the ductility and strain rate sensitivity of fabricated MMCs needs to investigated.

1.2 Research objectives

The main objective of this study is to investigate the high temperature mechanical behavior of aluminum and magnesium alloys after FSP. This goal is achieved through the following phases.

- Designing an effective experimental setup, including the fixture and FSP tools with different configurations to conduct friction stir processing.
- Investigating the influence of different FSP parameters on the resulting strength and ductility.
- Investigating the effect of embedding SiC reinforcements in the aluminum and magnesium alloys metal matrix via FSP on the mechanical properties of fabricated MMCs.
- Investigating the high temperature tensile behavior of processed materials and fracture mechanisms of samples.

1.3 Work summary

In the current study, friction stir processing (FSP) is used for the synthesis of both aluminum and magnesium metal matrix composite (MMC) reinforced by SiC particles. Microhardness enhancement were observed significantly for both Al2024/SiC and AZ31/SiC MMCs. Isothermal uniaxial tensile tests were employed for the as-received, friction stir processed and composite microstructures at ambient and high temperatures under strain rates ranging from 0.01 to 0.0001 s^{-1} to investigate the effect of deformation rate on the mechanical behavior. In case of Al2024 at ambient temperature, notable improvement of the yield

strength was observed reaching about 240% of the as-received samples while the ductility was reduced near to 4%. Also the notable improvement of ductility achieved for FSPed AZ31 sample.

For Magnesium based materials, in order to see the effect of high temperature under different strain rate on the grain size, microstructure of samples was observed for all different condition of annealed, FSPed and MMC after high temperature tensile tests. Elevated temperature flow curves were perceptibly sensitive to strain rate and for each case the strain rate sensitivity (m value) were calculated. Fracture surface observations hinted at the distribution of second phase particles along with possible damage mechanisms.

2 BACKGROUND AND LITERATURE REVIEW

2.1 Severe Plastic Deformation (SPD)

One of the most important microstructural factors is grain size which is affecting nearly all aspects of the chemical, physical and mechanical behavior of polycrystalline light alloys. The effect of grain size on the mechanical properties of materials is very complicated since the grain boundaries may possibly either act as obstacles to dislocation slip (strengthening effect) at ambient temperature or play a vital role to deform the material (softening effect) at elevated temperatures [1, 2].

Generally, the flow stress σ at ambient and low temperature depends on the grain size according to the Hall-Petch relationship [3, 4].

$$\sigma = \sigma_0 + k/d^{\frac{1}{2}} \quad (1)$$

where σ_0 is friction stress and *k* and *d* are the Hall-Petch coefficient and mean diameters of grains respectively. So many studies have been conducted to observe the validity of Hall-Petch relationship and experimental results of yield stress and grain size and in most cases the good agreements have been achieved [5, 6]. Severe Plastic Deformation (SPD) is a relatively new metal forming technology utilized to enhance the grain size of different coarse grained metals (e.g. titanium, aluminum, copper, magnesium, etc.) and produce an ultrafine

grained (UFG) material [7-9]. The capability of synthesis the non-structure bulk and sheet materials in the SPD process is the main factor of developing this method in different forms.

In the past three decades, various types of SPD methods such as equal channel angular pressing (ECAP) [10, 11], repetitive corrugation and straightening (RCS) [12], accumulative roll-bonding (ARB) [13, 14], severe torsion straining (STS) [15], high pressure torsion (HPT) [16], constrained groove pressing [17], cyclic extrusion compression (CEC) [18] and friction stir processing (FSP) [19] have been developed. ECAP, ARB, HPT and FSP techniques are well-investigated not only for fabricating ultra-fine grained structure materials but also to achieve the grain boundaries with high angle mis-orientation.

2.2 Pure aluminum and aluminum alloys

Pure aluminum is a soft, nonmagnetic and ductile metal which is makes up about 8% mass of the earth's crust. It is the third most abundant element after oxygen and silicon and the most plentiful metal in the crust, though it is less common in the bottom layers. as opposed to metals such as silver and gold, pure aluminum never found in nature. Instead, it forms compounds with other elements and to reveal the pure aluminum, compounds must be refined. One of those compounds is Bauxite which is mostly aluminum hydroxide (Al_2OH_3), made from about two-thirds alumina (aluminum oxide; Al_2O_3) and about a quarter water. Bauxite also have other compounds, like titanium oxide (TiO_2) and silica (SiO_2) [20]. The process of refinement needs money and energy but because of the important applications of aluminum this process is valuable and economic.

There are 14 different types of crystal unit cell structure or lattices but the unit cells favored by metals are the face-centered cubic (FCC), body-centered cubic (BCC) and

hexagonal close-packed (HCP) structures. Unit cell structure of aluminum is FCC which is shown in Figure 2.1 [21].

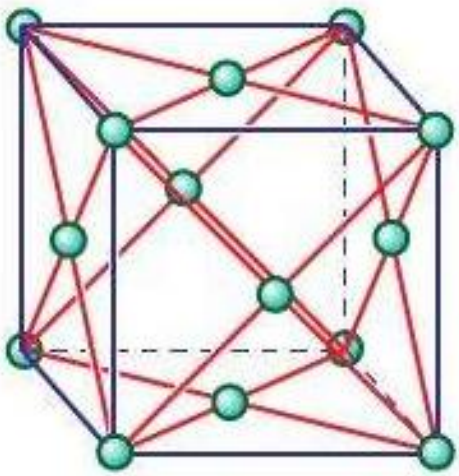

Figure 2.1 Schematic of Face-Centered Cubic (FCC) unit cell

Aluminum alloys are classified by International Designation System (IADS), depending on the classification established by Aluminum Association of the United States. There are two main classification of aluminum alloys; classification of wrought aluminum alloys and classification of cast aluminum alloys [20].

Wrought aluminum alloys are described by four-digit number. The first digit specified the alloy group as regards the principal alloying element. Principal alloying elements are added to the aluminum alloy and these are utilized to classified the aluminum series such as; 1000 series, 2000 series, 3000 series, up to 8000 series [22]. As it shown below, Table 2.1 depicts the classification of wrought aluminum alloys with a brief explanation of their properties and applications [20, 22, 23].

Table 2.1 Classification of wrought aluminum alloys

Alloy Series	Principal Alloying Element	Definition and Properties
1xxx	99% minimum Aluminum	Controlled pure aluminum alloys, this series are generally used in the electrical and chemical industries.
2xxx	Copper	The 2xxx series aluminum alloys, which is the major alloying element of copper, is generally used in the aviation industry due to its high yield strength as high as 455 MPa.
3xxx	Manganese	Utilized as general-purpose alloys for building industry and other numerous products.
4xxx	Silicon	Silicon is the principal alloying element and 4xxx series are utilized as welding rods and brazing sheet. Silicon addition range from 0.6 to 6.2%.
5xxx	Magnesium	5xxx series are the aluminum/magnesium alloys which are magnesium addition range are 0.2 to 6.2%. This series has high weldability so they are used for different applications.
6xxx	Magnesium and Silicon	Aluminum/magnesium and silicon alloys have 1% magnesium and silicon additions. These additions produces magnesium-silicade which is ensures the ability to become solution heat treated for enhanced strength.
7xxx	Zinc	Zinc addition range is 0.8 to 12%. 7xxx series are contain highest strength aluminum alloys. These alloys are utilized in aircraft, aerospace and sporting equipment applications.
8xxx	Other Elements	This series contains iron, lithium or tin.

2.3 Al2024 aluminum alloy

The aluminum-copper alloys usually contain between 2 to 10% copper, with smaller additions of the other alloying elements. The copper makes substantial increases in strength and facilitates precipitation hardening [24]. In the negative side, introduction of copper to aluminum is reducing the ductility and corrosion resistance. The major alloying elements of Al2024 copper and magnesium and generally used in aerospace industry as an important material for structural parts like fuselage of aircrafts because of high strength to weight ratio [25].

2.4 Pure magnesium and magnesium alloys

Magnesium is a rare shiny gray metal, bears a close physical resemblance to the rest of the alkaline earth metals, placed in the second column of the periodic table. As it shown in Figure 2.2 structure of magnesium is hexagonal close-packed (HCP) and ABAB stacking layers arranged in the unit cell. HCP structure of magnesium with atomic diameter of 0.32 nm is made it a favorable selection for solid solution with the other types of metals. Also the most pleasing properties of this metal is the low density of 1.738 $g.cm^{-3}$ which is nearly two-thirds of aluminum and makes it practically the lightest structural metal [26, 27].

Restriction of slip systems due to the crystal structure of magnesium caused to the difficult working of deformation mechanisms at ambient temperature then the results of mechanical properties of pure magnesium are not satisfactory as a structural material. With the purpose of strengthening the mechanical properties of pure magnesium different types of method are applied and alloying was the primary step of this process. Also the other strengthening methods such as grain refinement and precipitate hardening can be applied for

magnesium with using different methods like ageing and severe plastic deformation (SPD) techniques.

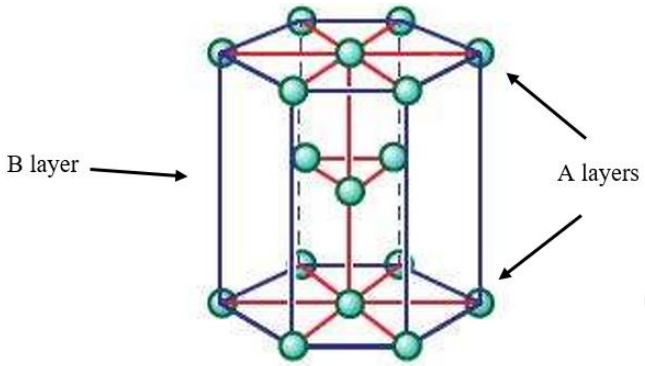

Figure 2.2 Schematic of hexagonal close-packed (HCP) unit cell

According to the American Society for Testing Materials (ASTM), the description of magnesium alloys is made by including letter codes of two major elements at first part and the nominal weight percentage of the composition of those elements at the second part [26]. For example, ZK21 is a magnesium alloy containing approximately 2% zinc and 1% zirconium. Table 2.2 shows the letter codes and examples of used magnesium alloys.

Table 2.2 Example of letter codes for magnesium alloys

Letter code	Elements	Examples	Composition (wt.%)
A	Aluminum	AZ31	3Al-1Zn
C	Copper	ZC63	6Zn-3Cu
Z	Zinc	ZK60	6Zn-0.5Zr
K	Zirconium	K1A	0.7Zr
M	Manganese	AM60	6Al-0.13Mn
S	Silicon	AS41	4.3Al-1Si

2.4.1 Effect alloying elements on the properties of magnesium alloy

Solid solution strengthening is the most achievable types of strengthening for magnesium alloys due to the appropriate atomic diameter matching with the alloying elements like aluminum and zinc. Atomic mismatch with magnesium for aluminum is approximately 13% and for zinc, it is less than 9%. The current study focuses on AZ31, hence the effect of the aluminum and zinc in magnesium is briefly described.

According to the Figure 2.3a, the maximum level of solubility for aluminum in magnesium is 12.7 wt.%. One of the most important advantage of adding the aluminum is improving the castability of magnesium alloys due to the enhancement of the fluid flow of the melt [28]. Elseways, extra addition of aluminum rises the risk of shrinkage throughout casting. The solubility of aluminum at ambient temperature drops to 2 wt.%. Therefore, brittle $Mg_{17}Al_{12}$ precipitates will form decreasing the mechanical strength. $Mg_{17}Al_{12}$ locates on the basal slip planes and has not any effect on obstructing the movement of basal dislocations. During age hardening, it forms in long lath shaped particles which also decline the mechanical strength [29].

Zinc is also the second important alloying element in AZ alloys and as it is shown in Figure 2.3b, the maximum level of solubility of this element is magnesium matrix is 6.2wt.%. The addition of zinc increases the melt fluidity as well as the critical resolved shear stress (CRSS) on the basal planes attributed to the solid solution strengthening method. Even though CRSS value is increased for basal slip, more addition of zinc declines the CRSS on prismatic slip leading to better ductility [30].

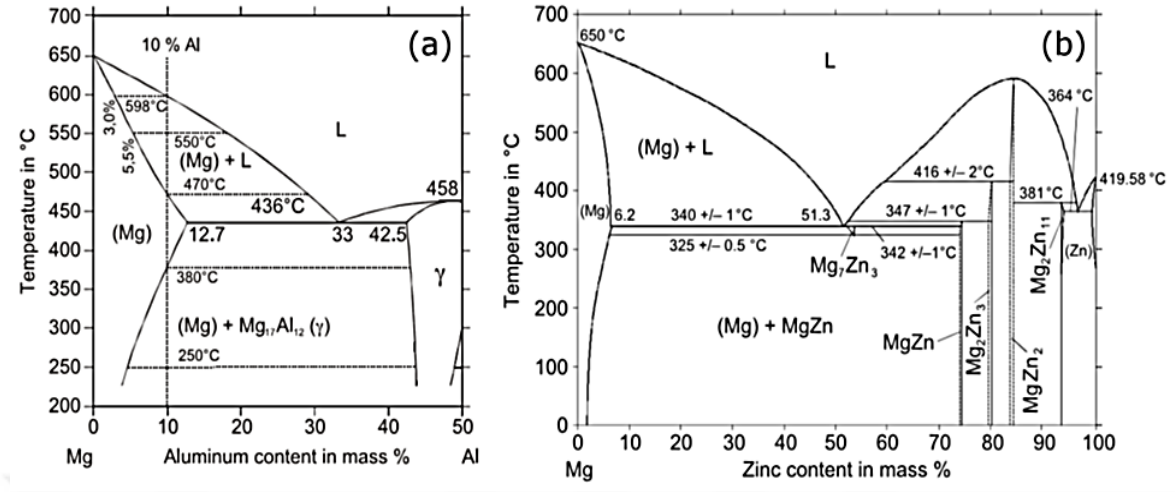

Figure 2.3 Binary phase diagrams of (a) Mg-Al and (b) Mg-Zn [31].

2.4.2 AZ31 magnesium alloy

One of the most applicable and structural magnesium alloys are aluminum-zinc-manganese, which are termed by AZ letter codes. AZ series are mostly used where good castability and high strength are required. The mechanical properties of the AZ group decreases promptly at high temperature above 120°C attributed to the fact that magnesium alloys undergo creep mainly by grain boundary sliding. In the other hand, $Mg_{17}Al_{12}$ precipitates exists in the as-cast condition of the AZ series of magnesium alloys and after heat treatment of these series up to 420°C, aforementioned phase dissolves in the solution. Solid solution strengthening method adds to the strength of the matrix while the existence of this precipitate drops the ductility of these magnesium alloys [32].

AZ31 magnesium alloy is commercially accessible in sheet form, and offers relatively good mechanical properties. Inappropriately, the low ductility, around 12% at room temperature, and also the brittle-like behavior of mentioned alloy is limited its application

[33]. However, limited researches have been done to increase the formability of AZ31 at elevated temperatures and even achieve superplastic behavior [34, 35].

2.5 Deformation systems in magnesium alloys

Unlike cubic metals, the hcp structure is limited the deformation mechanisms of magnesium at room temperature and decreased the ductility of these types of materials. Whenever additional slip systems would be activated, high ductility can be achieved specifically at high temperatures [36]. Deformation mechanisms of magnesium alloys are mainly dominated by slip system at room temperature. Nevertheless, twinning also contributed when slip systems are inadequate. In the other hand, the primary deformation mechanism of magnesium alloys at elevated temperatures is grain boundary sliding (GBS) [37].

2.5.1 Slip systems

Movement of blocks of crystals along the satisfactorily oriented planes of crystals is termed slip. In single crystals there are favored planes where dislocations move (slip planes). There they do not move in any way, but in desired crystallographic directions (slip direction). The set of slip planes and directions create slip systems. But dislocation movement normally happens along the closed-packed crystallographic orientation known as slip direction with a plane which have the highest atomic density. Slip systems are labelled with the combination of these slip directions and slip planes [38]. The highest atomic density in the magnesium structure is for (0001) plane (basal plane), and the closed packed direction is {11-20}, then the most possible slip occurs on the basal plane along the {11-20} direction. Figure 2.4 depicts slip systems and twinning in for an hcp crystal of magnesium.

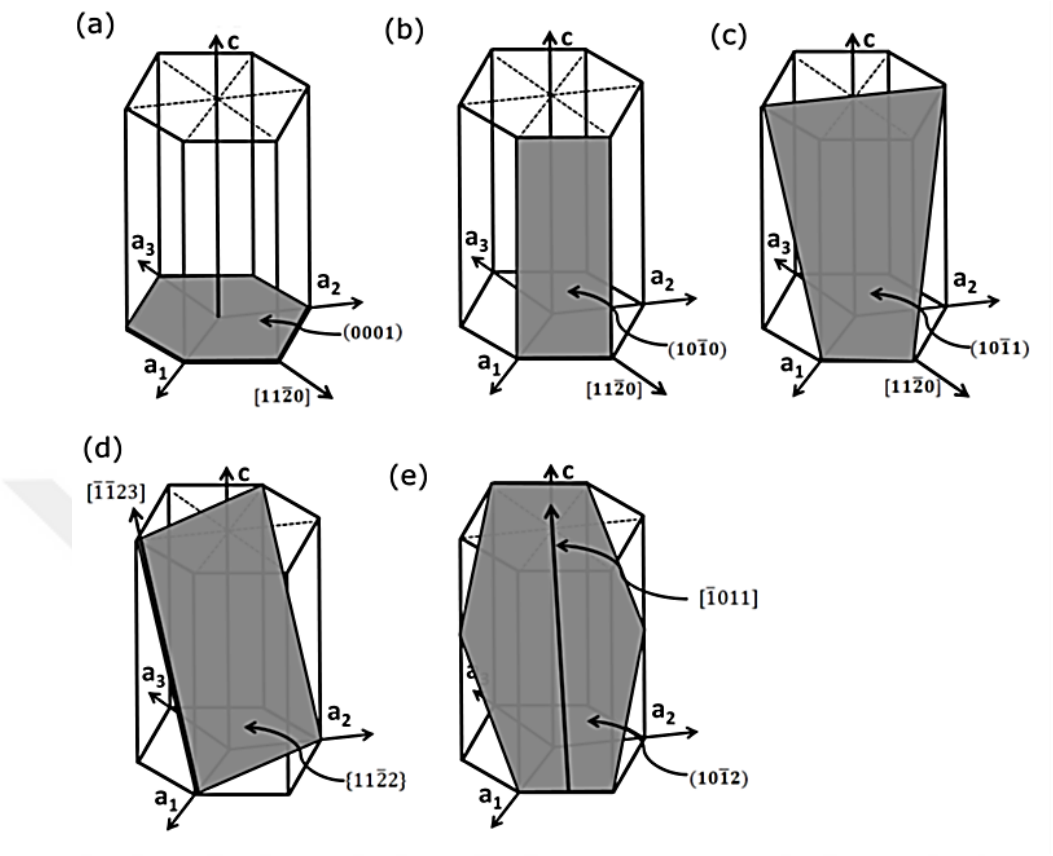

Figure 2.4 Slip and twinning systems in an hcp crystal (a) basal (0001) {11-20}; (b) prismatic (10-10) {11-20}; (c) first order pyramidal (10-11) {11-20}; (d) second order pyramidal (11-22) {1123} slip systems and (e) tension twinning (10-12) {10-11}.

2.5.2 Twinning

The symmetric orientation of blocks of unreformed crystals produced by the deformation of a portion of deformed crystals is named twinning [38]. Figure 2.5 shows the difference between the slip and twinning deformation.

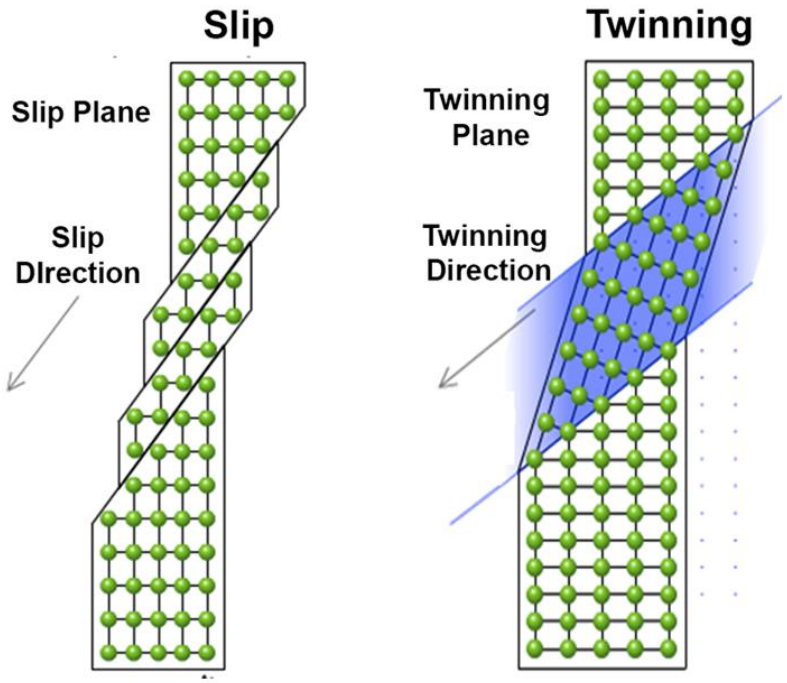

Figure 2.5 Schematic of slip and twinning deformations [39].

2.6 Metal Matrix Composites (MMCs)

Recently there is a surge in research on the mechanical behavior of metal matrix composites (MMCs) because of their advanced physical and mechanical properties, such as high elastic modulus, and strength, these advantages can make them the most attractive candidate materials for automotive, aerospace and other applications [40-42]. Combination of metallic features, such as ductility and toughness with the high strength, high modulus refractory ceramic materials in MMCs leads to higher strength in compression and shear [43]. High strength-weight ratio is one of the most critical aspects of material selection in aviation industry and with respect to this criteria, MMCs became a favor substitution for

conventional materials. For example, replacing wrought aluminum alloy with the SiC reinforced one of that, resulted the 50% rise in strength and 10% decrease in weight [44].

The most common types of reinforcements which are used in composites are filler reinforcement, random-fiber or short-fiber reinforcement, long-fiber reinforcement, flake reinforcement and particulate reinforcement. In spite of the satisfactory results of fiber reinforced metal matrix composites, wide industrial application of mentioned materials has been hindered because of the high fiber reinforcements cost and expensive manufacturing process [43].

Additionally, continuous fiber reinforced composites usually have not the capacity of secondary forming process and the application of these composites are limited with this problem [45, 46]. Unlike the fiber reinforcements, low cost of particulate reinforcements and accessibility of different types of them has attracted significant attention to fabrication of MMCs with these particles.

Particulate reinforced composites are typically classified by the type of reinforcement they use. This reinforcement is embedded into a matrix that holds it together. The reinforcement materials are utilized to strengthen the composite and include different types such as oxides (SiO2, Al2O3) [47, 48], nitrides (AlN4, Si3N4) [49, 50] and the most popular one carbides (SiC, B4C, TiC, WC) [51-54] as well as elements like silicon [55] and carbon [56]. MMCs receive a considerable share since reinforcement with secondary particles could lead to high strength, high elastic modulus, and improved resistance to wear, corrosion, creep and fatigue making them decent structural materials for aerospace and automobile components. Nevertheless, these composites may also lose ductility and toughness attributed to the incorporation of non-deformable ceramic reinforcements, limiting their scope [57].

Different manufacturing process are available for production of particle reinforced MMCs such as Liquid metallurgy (stir casting), Squeeze casting, Powder metallurgy, Spray casting, Lanxide technique. Also recently so many surface modification methods such as high-energy electron beam irradiation [58, 59], plasma spraying [60], high-energy laser surface engineering [61, 62], cast sinter [63] and friction stir processing (FSP) [64, 65] have employed to produce surface metal matrix composites.

2.7 Friction Stir Processing (FSP)

Friction stir processing (FSP) has been developed by Mishra et al [66-68] for microstructural modification and then recently this technique is applied for embedding ceramic particles inside of the surface metal matrices and also for surface modification of MMCs. The basic principles of FSP are similar to the friction stir welding (FSW) which is relatively novel joining method developed by the Welding Institute (TWI) of UK [69]. FSW was invented as a solid-state joining method with primary application to aluminum alloys and later on to other non-weldable light alloys like copper, nickel, and titanium [70-72]. In addition to surface modification, severe plastic deformation (SPD) during FSP has led to many applications such as grain refinement of coarse-grained materials [73-76], homogenization of cast alloys [77, 78], powder metallurgy parts [79] and both fabrication and homogenization of MMCs [80-82]. Figure 2.6 depicts the schematic drawing of the FSW process which is similar to the friction stir processing with the substitution of nugget zone with the term of stir zone.

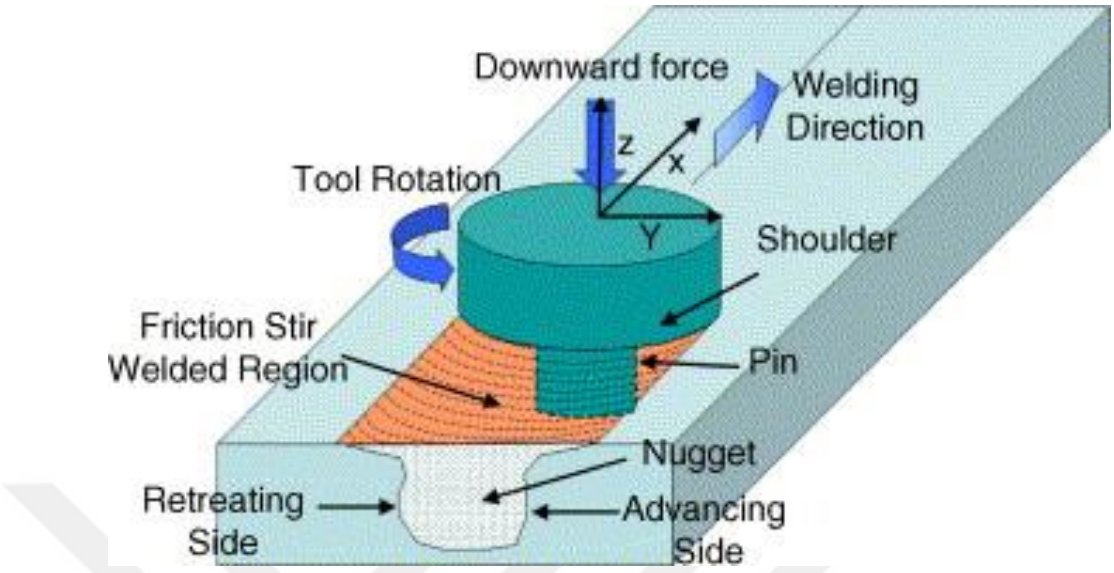

Figure 2.6 Schematic design of friction stir welding [83]

FSP has great advantages including: solid-state microstructural evolution, adjusting mechanical properties by optimizing tool design and process parameters, the depth of processed zone and location which can be identified by the operator. Moreover, the process does not produce any deleterious gas, noise and materials distortion. MMCs which are manufactured by FSP have good advantages, such as high strength, high elastic modulus and also better surface performance like higher wear resistance and hardness [84]. However, these composites suffered from low ductility and toughness due to incorporation of ceramic reinforcements, which limited their wide applications to a certain extent. Generally surface properties determined the useful life of components where wear and fatigue resistance were main concern. In these situations, only surface layer of components was reinforced by reinforcement particles while the bulk of component retained the original properties.

Su et al. [85] have investigated the effect of combining FSP with rapid cooling on the microstructure of Al7075 aluminum alloy. They successfully produced ultra-fine grain

samples with grain size of 100, 180, 300 and 500 nm with controlling cooling rate. They have found that high cooling rate positively affected on grain refinement of Al7075 with forming the high-angle grain boundaries in attributed to the high temperature discontinuous dynamic recrystallization.

Recently, Darras et al. [33] have investigated the microstructure evolution commercial AZ31 magnesium alloy with using friction stir processing technique. Figure 2.7 illustrates the effects of two key parameters of FSP on the temperature of plate during the process. Figure 2.7a depicts that increasing the tool rotational speed from 1200 rpm to 2000 rpm, at the constant traverse speed of 560 mm/min increased the maximum temperature of workpiece from 450˚C up to about 580˚C. On the other hand, as demonstrated in Figure 2.7b, at the constant rotational speed of 1200 rpm, with raising the traverse speed from 508 mm/min to 762 mm/min the peak temperature of plate enhanced up to 480˚C.

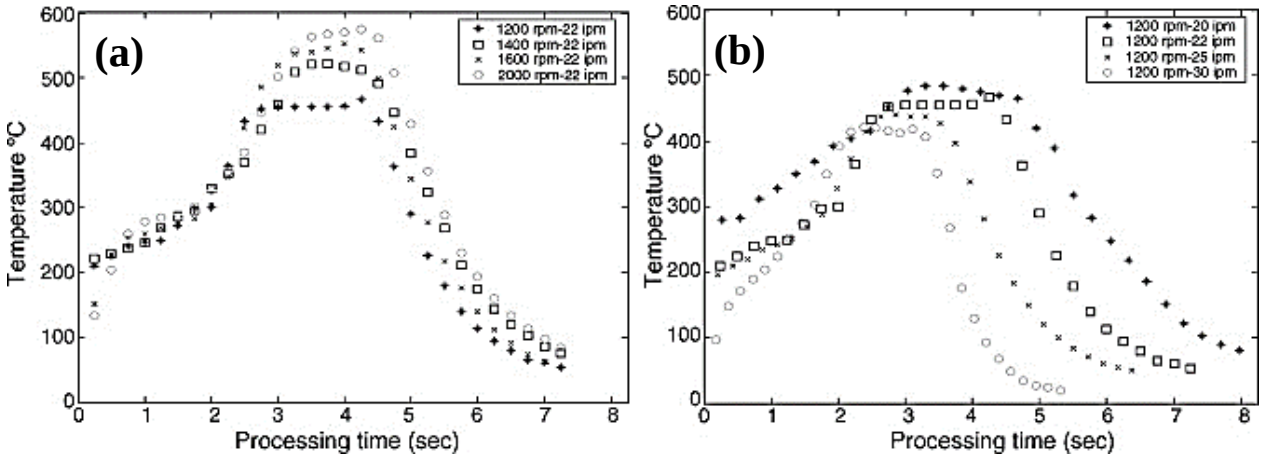

Figure 2.7 Effect of rotational speed and traverse speed on the peak temperature of plate during the process[33].

Zongyi Y. Ma et al. [86] studied the effect of tool rotational speed and traverse speed through FSP on the grain refinement and uniformity of grains and completely eliminated the

porosity and voids of the A356 Aluminum alloy. Additionally, they reported that higher rotation speed generates a more homogeneous microstructure and refined the grains to the average size of 3-4 μm.

Effect of peak temperature, cooling and heating rate on the tensile properties and microstructure evolutions of AZ31 magnesium alloy during the FSP was investigated by Darras et al. [87]. They found that formability AZ31 Magnesium alloy can be improved by FSP. As illustrated in Figure 2.8 significant increase in the elongation was achieved (up to nine times when FSP in hot water).

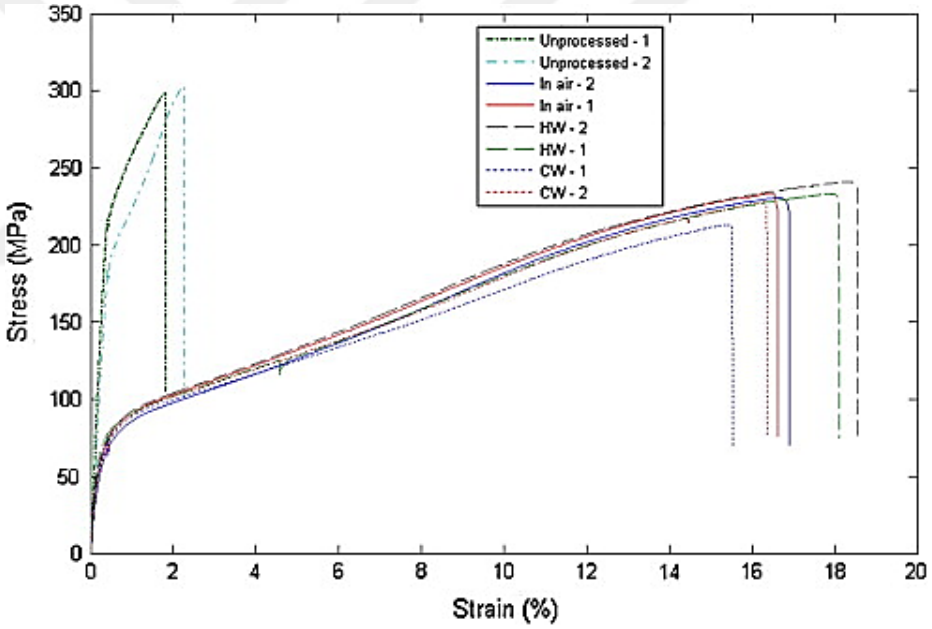

Figure 2.8 Stress–strain curves for unprocessed, FSP in air, submerged in hot water and submerged in cold water [87].

2.8 Metal matrix composites fabricated by friction stir processing

As in mentioned in previous sections, friction stir processing can be a preferable fabrication methods of metal matrix composites but the lack of investigation about bulk mechanical

properties like yield and ultimate strength, ductility, toughness and fatigue behavior of MMCs fabricated by FSP is limited the application of this method.

Recently, concentration of researches on the mechanical properties of the MMCs are increased and many investigations have been done to observe the effect of process parameters and characterization of them to achieve the best and optimum properties.

2.8.1 Aluminum MMCs fabricated by friction stir processing (FSP)

The Al5083/SiC surface composites with dissimilar volume fractions of reinforcements were successfully fabricated using FSP method by Mishra et al. [88]. The SiC reinforcements were uniformly distributed in the matrix and excellent bonding was observed between surface composite and aluminum alloy substrate. Also they reported the significant enhancement of microhardness from 85 Hv of Al5083 alloy substrate up to 173 Hv for surface composite reinforced by 27 vol. % SiC with average particle size of 0.7 μm.

Alidokht et al. [89] successfully incorporate premixed MoS_2 and SiC particles into the A356 aluminum alloy in order to fabricate the hybrid composite via FSP. They reported that wear resistance of the processed materials enhanced considerably as compared to that of the as-cast alloy. Uniform distribution of reinforcements and a MoS_2 mechanically mixed layer (MML) observed inside the stirred zone and on the top of worn surface respectively. Aforementioned layer of MoS2 improved tribological properties of the alloy composite attributed to stifle plastic deformation.

Y. Morisada et al. [90] successfully dispersed Fullerene into A5083 aluminum alloy by FSP and they observed that dispersion of the fullerene improved the grain refinement benefits recrystallization through the FSP. They reached the ultrafine grain size of 200nm and enhanced the hardness affected by both grain refinement and dispersed fullerene.

Aruri et al. [91] have made an investigation about the effect of tool rotational speed on the wear and mechanical properties of aluminum based hybrid composites fabricated by FSP. They observed that the SiC, Gr and Al_2O_3 particles were uniformly dispersed in the stirred zone. They also found that the microhardness declines when increasing the rotational speed and exhibited higher microhardness value in Al–SiC/Al2O3 hybrid composite attributed to existence and pining effect of hard SiC and Al2O3 reinforcement.

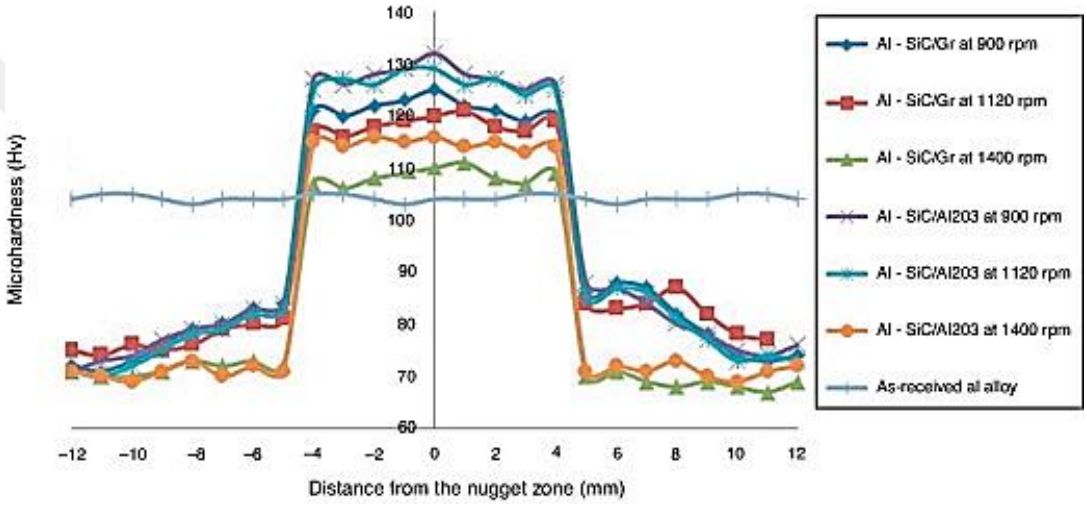

Figure 2.9 Microhardness of aluminum based surface hybrid composites [91].

Influence of FSP parameters such as tool rotational speed, traverse speed, number of FSP passes, shift of rotational direction between passes and particle size during the manufacturing process Al5052/SiC MMC on distribution of SiC particles in metal matrix, microstructure, microhardness and wear properties of specimens was investigated by Dolatkhah et al. [92]. They found the optimum parameters for achieving desired powder dispersion in MMC and results demonstrated that increase in number of passes, change of tool rotational direction between FSP passes and reduction of SiC reinforcements size

improve hardness and wear properties. However, the bulk mechanical properties of MMC such as yield and ultimate tensile strength, ductility and fatigue were not studied.

2.8.2 Magnesium MMCs fabricated by friction stir processing (FSP)

M. Balakrishnan et al. [93] applied FSP method to produce the AZ31/TiC MMC with different volume fractions of TiC powder. The results indicated that TiC particles were distributed uniformly in the magnesium matrix without the formation of clusters. There was no interfacial reaction between the magnesium matrix and the TiC particle. TiC particles were properly bonded to the magnesium matrix.

S. Das et al. [94] were used multiple passes FSP to make magnesium WE43/ B4C MMC (WE43 is a magnesium alloy) with adding B4C powder with particle size of 6μm and they found that hardness and elastic modulus were improved 19% and 41% respectively.

Multi-walled carbon nanotubes (MWCNTs) were successfully dispersed by Y. Morisada et al. [95] into AZ31 using friction stir processing (FSP). Distribution of the MWCNTs was changed on the basis of the travel speed of the FSP tool. The grain size of the MWCNTs/AZ31 surface composites was smaller than that of the FSPed AZ31 without the MWCNTs. The maximum microhardness of these composites was 78 Hv, which is almost double that of the AZ31 substrate (41 Hv).

Effect of rotational speed and probe profile on microstructure and hardness of AZ31/Al2O3 nanocomposites fabricated by friction stir processing is investigated by Azizieh et al. [96] and they reported that by increasing the rotational speed, as a result of greater heat input, grain size of the base alloy increased and simultaneously more shattering effect of rotation, cause a better nanoparticle distribution. The average grain size of matrix of the composites was in the range of 1–5 μm and the microhardness of them was 85–92 Hv.

C.Y.H. Lim et al. [97] investigated the wear behavior of magnesium (Mg)-based metal matrix composites (MMCs) reinforced with silicon carbide particles (SiCp) during dry sliding and the composite exhibit slightly superior wear resistance under the lower load, but the effects of SiC particulate reinforcements on wear resistance are not as conclusive under higher load. During SEM analysis, it was observed that the melt wear becomes the dominant wear mechanism, causing gross deformation of the magnesium matrix at the contacting interface. The useful range of Mg/SiCp composites appears to be limited to loads and speeds below 30 N and 5.0 m/s respectively.

2.9 High temperature mechanical behavior of metal matrix composites after FSP

Very limited researches, investigating the high temperature mechanical properties of the MMCs fabricated by FSP are available. P. Cavaliere have done a worthy research about the fabrication of Al2618/Al_2O_3 MMC via FSP, and investigating the superplastic properties of processed materials. As shown in Figure 2.10, he investigated the high temperature tensile behavior of the fabricated composite at different strain rates, and the results illustrates that the flow stresses are increasing with raising the strain rates at each constant temperature. Also the fracture surfaces of fatigue test samples were observed and they found the fracture caused by the cracking the base material microstructure accompanied with the failure of Al2O3 particles and separation at the particles–matrix interfaces [47].

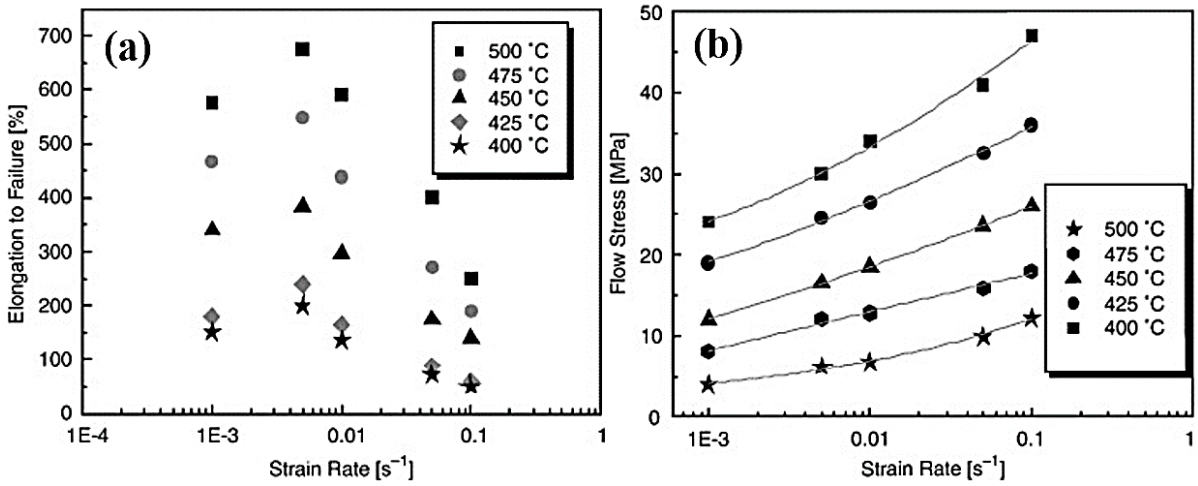

Figure 2.10 (a) Total elongation to failure of Al2618/SiC MMC as a function of the different strain rates and different high temperature tests (b) Flow stress level of Al2618/SiC MMC as a function of strain rate at all the testing temperatures [47] .

Also C.J. Lee et al. [98] have investigated the effect of embedding nano-sized SiO_2 into the AZ61 Magnesium alloy via FSP on the microstructure evolution and high temperature tensile behavior. They found that tensile elongation of fabricated nanocomposite reached to about 400% at 350˚C under the high strain rate of 0.1 s^{-1}, clearly exhibiting high strain rate superplasticity (HSRSP). However, the tensile elongation at the same temperature under strain rate of 0.001 s^{-1} was almost 100%.

3 EXPERIMENTAL METHODS

3.1 As received material's characterization and initial preparation details

3.1.1 Al2024 aluminum alloy

Al2024 sheets with the thickness of 3 mm were used for FSP. The as-received material were received in the annealed condition. The chemical composition of commercial Al2024 aluminum alloy is given in Table 3.1. Al2024 slabs were cut by wire cut electro-discharge machining (EDM) with dimensions of 120×55×3 mm.

Table 3.1 Chemical composition of Al2024

Element	Cu	Mg	Mn	Fe	Si	Zn	Ti	Al
wt.%	4.8	1.49	1.49	0.12	0.08	0.04	0.036	Balance

3.1.2 AZ31 magnesium alloy

The as-received material used in this section was a commercially called AZ31 magnesium alloy. The chemical composition of AZ31 slab which is used in this study is summarized in Table 3.2.

Table 3.2 Chemical composition of AZ31

Element	Al	Zn	Mn	Cu	Si	Fe	Mg
wt.%	3.23	2.43	0.79	0.77	0.16	0.11	Balance

AZ31 slabs were cut to the dimensions of 120×45×3 mm with using EDM in order to prepare them for process. Prior to the applying FSP on the magnesium alloy slab, Annealing treatment was performed on the as-received AZ31 at 400°C for 3 hours inside vacuum furnace and pressure was decreased to 10^{-3} mbar using vacuum apparatus in order to prevent the oxidation of magnesium slabs (Figure 3.1). This treatment was necessary not only for removing the effect of previous heat treatment but also for homogenizing the microstructure of as-received AZ31.

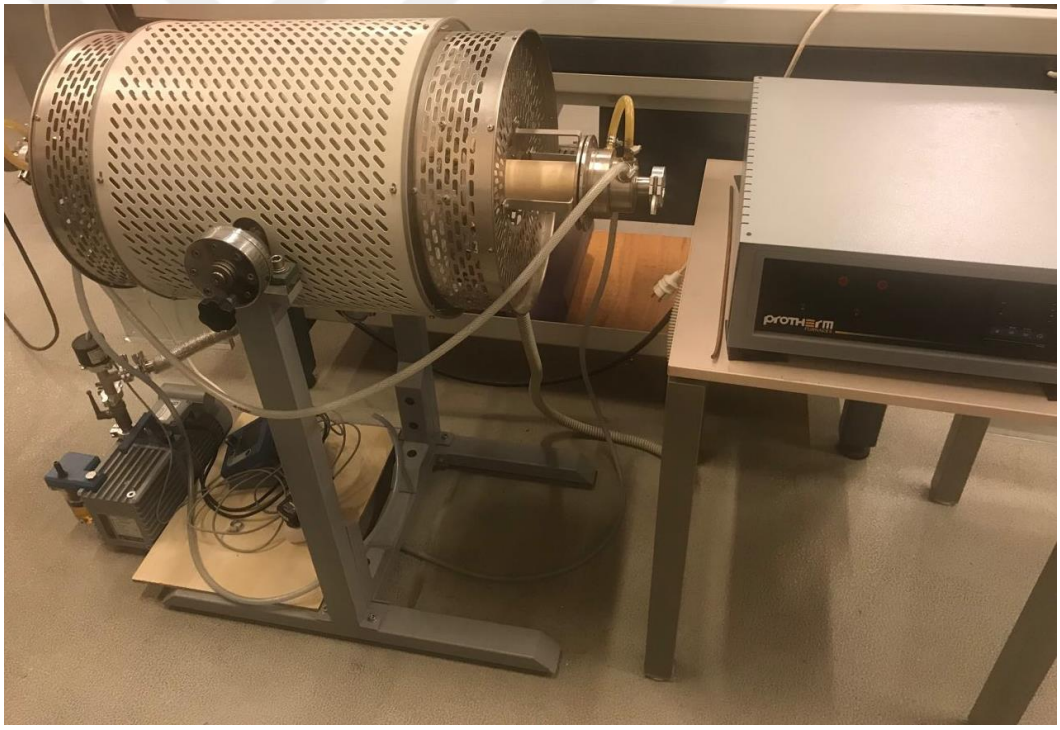

Figure 3.1 Vacuum furnace.

3.2 Design of the fixture

Figure 3.2 illustrates the fixture which is used for this study for friction stir processing of both Al2024 and AZ31. There are two fillers at both sides of the workpiece in order to prevent the movement of the sheet.

Figure 3.2 Friction stir processing fixture

3.3 Design of the plate and FSP tool

As it shown in Figure 3.3, holes and groove included plates were designed in order to put the SiC particles in side of the metal matrix. These two designs were selected based on the previous works [99] and then after completing the preliminary experiments the groove included plates were chosen for the current study. Although the uniformity of particles was satisfactory in case of plate with holes, the voids and porosities were observed inside of the matrix.

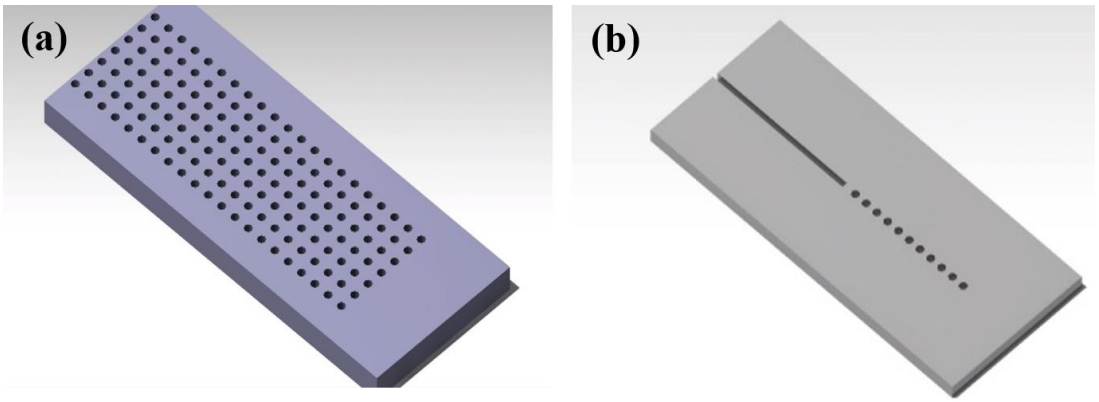

Figure 3.3 (a) plate with holes; (b) plate with Groove and holes designed for embedding the reinforcement particles.

Figure 3.4 demonstrates two different tools were designed and made for the current experiment. The pinless tool which is shown in Figure 3.4a was utilized as an initial process of FSP in order to close the surface of grooves and then the tool with rectangular shape pin were used to mixing the particles and embedding the reinforcements inside of the metal matrix. The pin shape selected based on the best results of particle distribution taken from the literatures [100, 101]. The dimensions of tool used in the present experiment had a shoulder diameter of 14 mm and a square pin with 5 mm edge length and 2.65 mm height.

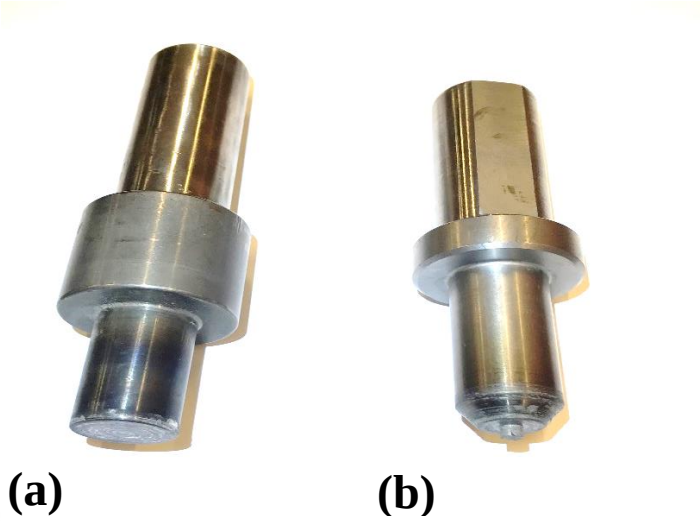

Figure 3.4 FSP tools (a) without pin (b) with pin.

3.4 Friction stir processing parameters

The FSP parameters were selected based on an experimental design incorporating an L9 orthogonal array test matrix with strength selected as the response factor [102, 103]. In case of Al2024, the parameters used in the campaign are listed in Table 3.3, among these the plates were processed at a tool rotational speed of 1600 rpm, traverse speed of 40 mm/min and plunge depth of 0.15 mm for gaining optimized strength. The fabrication method included repeated friction stir passes on the groove region, employing SiC particles with an average size of 4.5 µm.

Table 3.3 FSP parameter set.

Levels	Rotational Speed (rpm)	Traverse Speed (mm/min)	Plunge Depth (mm)
1	1200	30	0.15
2	1400	40	0.20
3	1600	50	0.25

3.5 Design of Experiment (DOE) based on the Taguchi's method

As it is listed in Table 3.4, an L9 orthogonal array test matrix with 3 parameters of rotational speed, traverse speed and plunge depth has been applied with the response factor of ultimate tensile strength (UTS), in order to decrease the number of experiments from 27 to 9 experiments. Aforementioned parameters were selected based on the results of the 9 tests as it shown in Figure 3.5.

Table 3.4 Al2024 FSP parameters based on the Taguchi method

Rotational speed (rpm)	Transverse speed (mm/min)	Plunge depth (mm)	UTS (MPa)
1200	30	0.15	300
1200	40	0.20	290
1200	50	0.25	255
1400	30	0.20	320
1400	40	0.25	320
1400	50	0.15	285
1600	30	0.25	370
1600	40	0.15	420
1600	50	0.20	315

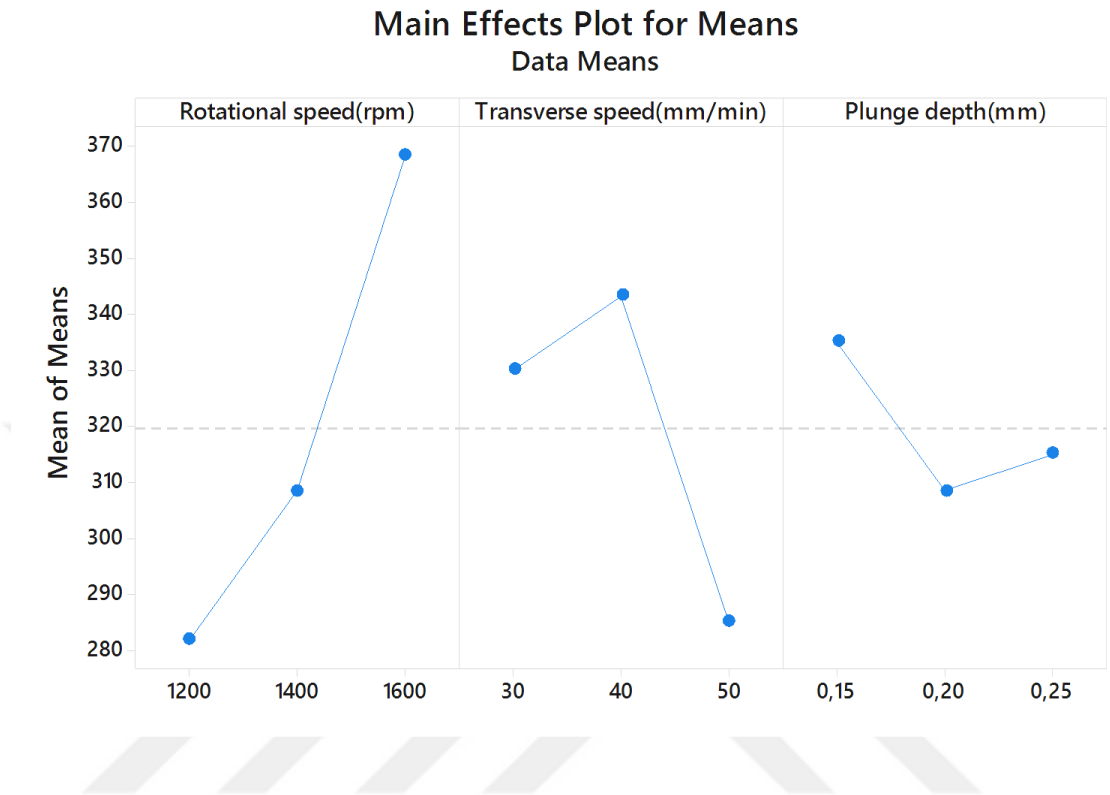

Figure 3.5 Taguchi's method for Al2024 FSP based on the UTS response factor.

The same procedure was used for friction stir processing of the AZ31 magnesium alloy and based on the preliminary experiments and also the results of other researches the best three levels for each parameter were taken in Table 3.5 and using Taguchi's method the optimum parameters for FSP was selected (Figure 3.6).

Table 3.5 AZ31 FSP parameters based on experimental design.

Rotational speed (rpm)	Transverse speed (mm/min)	Plunge depth (mm)	UTS (MPa)
1000	30	0.10	270
1000	60	0.15	315
1000	90	0.20	290
1200	30	0.15	315
1200	60	0.20	335
1200	90	0.10	295
1400	30	0.20	265
1400	60	0.10	305
1400	90	0.15	325

With respect to the Figure 3.6, it can be understood that increasing the plunge depth, rotational and traverse speed of tool caused the improvement of UTS and then decrease it. This trend can be attributed to the changing heat input during the experiment which is important factor to have a defect free processed material. Also the maximum temperature of plate is directly related to the rotational speed and traverse speed made it an important factor for the final grain size of FSPed and MMC [104-107]. Based on the results of the experiments, rotational and traverse speed of 1200 rpm and 60 mm/min were selected respectively, with plunge depth of the 0.15mm.

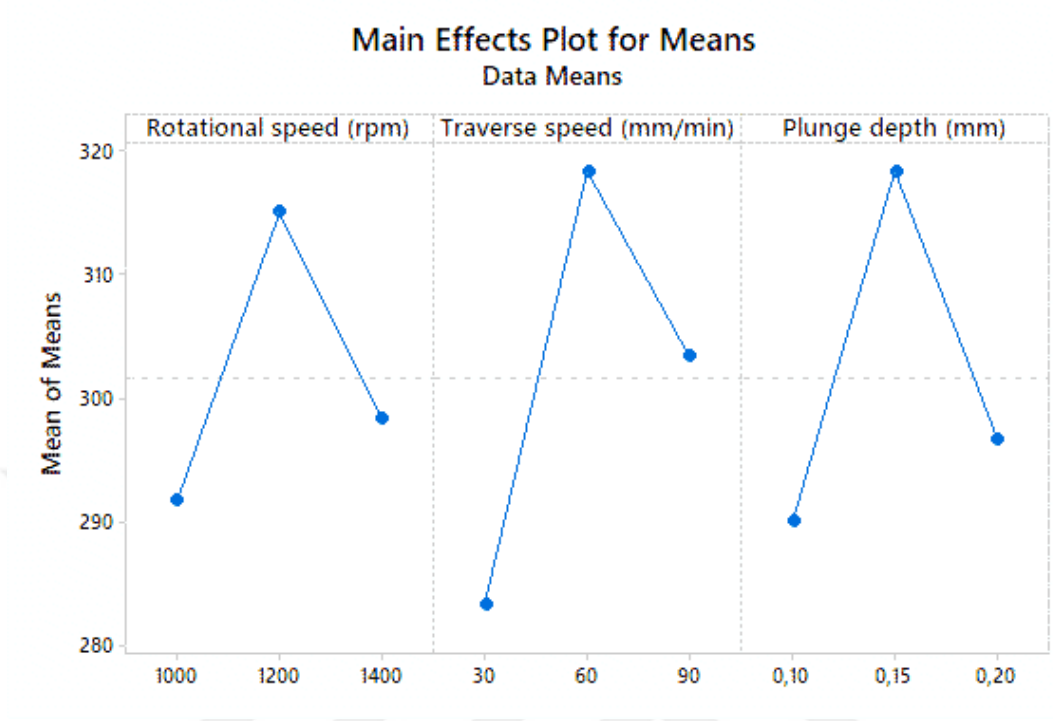

Figure 3.6 Taguchi's method for AZ31 FSP based on the UTS response factor.

3.6 Mechanical testing

3.6.1 Hardness measurement

E92 ASTM standard for hardness test was utilized to prepare the samples. The grinding process was conducted up to 2500 grits then the samples were polished using the 6, 3 and 1 µm diamond suspension. Microhardness of the samples after grinding and polishing was measured using a Vickers indenter with a force of 1000 gf for 15 s. To make sure about the accuracy and repeatability of the results, minimum three hardness tests were performed on every condition and the mean value of obtained results was reported. The standard deviation of values was determined to be lower than 5%.

3.6.2 Uniaxial tensile tests

In order to investigate the bulk mechanical properties of the processed samples, uniaxial tensile tests were conducted. In addition to ambient temperature tests, high temperature tensile tests at 300°C were applied to characterize the high temperature mechanical behavior of both Al2024 and AZ31.

Dog-bone shaped tensile samples have been cut using electro-discharge machining (EDM) with a gauge length of 15 mm. The samples were prepared in the tool traverse direction during the friction stir processing. In order to remove the effect of residual stress and scratches, all of the samples were ground and polished before the tests.

An Instron mechanical testing frame equipped with an environmental chamber was used. The specimen temperature was measured using K-type thermocouples during deformation. Also the displacement and consequently the strain value of the samples were recorded using an extensometer. Three different strain rates of 10^{-2}, 10^{-3} and 10^{-4} s^{-1} were selected to observe the strain rate dependency of materials at high and room temperature. Also the strain rate sensitivity (*m* value) was calculated based on the results of the tensile tests and flow behavior of the samples.

The high temperature tensile tests were conducted inside a furnace mounted to the Instron testing frame while the samples were heated up until reaching to the 300°C using the heaters attached to the guiding mills of the frame as shown in Figure 3.7, then delayed for 10 minutes to eliminate the temperature gradient inside of the sample. Finally, after finishing the tests samples were quenched in water for further fracture morphology analysis.

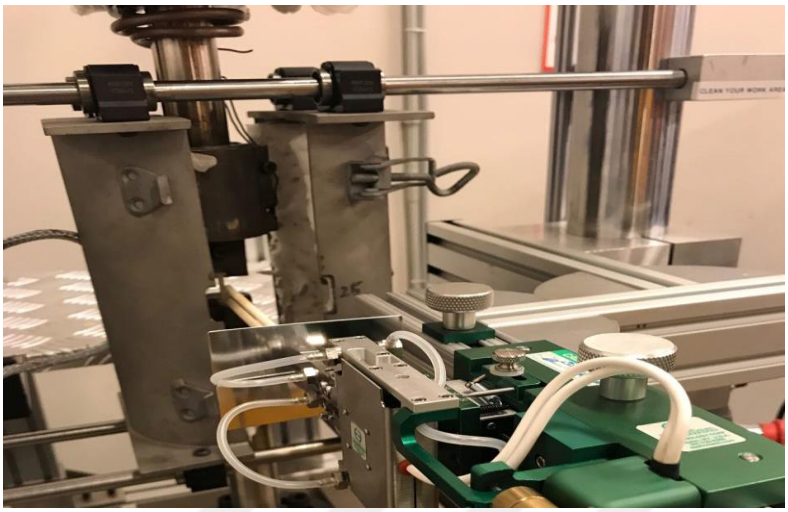

Figure 3.7 High temperature tensile test setup.

3.7 Microstructure Evaluation methods

3.7.1 Optical Light Microscopy

After completing the process samples were cut in to the small dimensions using the micro cutting machine then samples were cold mounted with using the mixture of resin epoxy and hardener.

Conventional metallographic preparation technique was applied. Grinding process using water as a lubricant in order to cooling and prevent the damage in microstructure were done with 500,800, 1200, 1500 and 2500 grits SiC papers.

Cloths of 6, 3 and 1 μm were used for polishing by diamond suspension. In case of the AZ31 samples, during polishing ethanol based lubricant was used to prevent surface scratching and particle surrounding into the magnesium matrix. Ground and polished samples were rinsed in ethanol and water after the operation. Then two different etching solution were provided for aluminum based and magnesium based samples. The Al2024 samples were

etched immersing in the Keller's reagent solution consisting of 95 ml water, 2.5 ml nitric acid (HNO_3), 1 ml hydrofluoric acid (HF) and 1.5 ml hydrochloric acid (HCl). On the other hand, the AZ31 samples were chemically etched in a solution of 5 gr picric acid, 10 ml acetic acid, 70 ml ethanol and 10 ml distilled water for 30 seconds to reveal grain boundaries. A microscope attached to the camera was employed to reveal the grains at different magnifications of 20x and 50x.

3.7.2 Scanning Electron Microscopy (SEM)

In order to observe the fracture morphology of different conditions for both magnesium and aluminum alloys, scanning electron microscopy (SEM) was applied. Scanning electron microscopy (SEM) studies aimed at investigating the fracture mechanisms and SiC particle distribution, were conducted in a ZEISS SEM equipped with an energy dispersive X-ray spectroscopy (EDS) detector at an accelerating voltage of 15kV (Figure 3.8).

Figure 3.8 ZIESS scanning electron microscope (SEM).

4 HIGH TEMPERATURE CHARACTERISTICS OF Al2024/SiC METAL MATRIX COMPOSITE FABRICATED BY FRICTION STIR PROCESSING

4.1 Microstructure and hardness characterizations

It can be followed from Figure 4.1 that FSP with SiC particles led to considerable grain refinement in the as-received condition. At the stir zone (SZ), the material is under severe plastic deformation (SPD) causing the formation of fine grains with high angle boundaries [108] and many locations for the nucleation of new grains can be revealed in the SZ [109, 110]. With respect to the grain refinement, the density of grain boundaries increased and the average grain size decreased from 22 μm down to 2.3 μm. Also schematic of different parts of FSPed sample includes base metal (BM), heat affected zone (HAZ), thermo-mechanically affected zone (TMAZ) and stir zone (SZ) are shown in Figure 4.1.

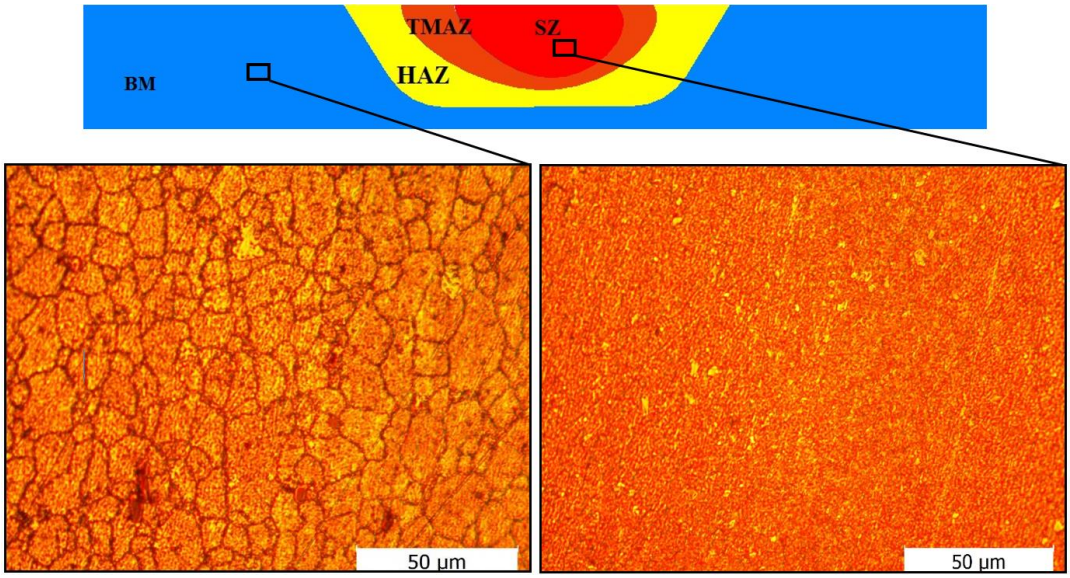

Figure 4.1 Microstructure of Al2024 (a) as-received; (b) the stir zone.

Figure 4.2 EDS analysis of the MMC sample from the (a) aluminum matrix and (b) SiC particle. shows the EDS analysis obtained on the as processed Al2024/SiC MMC sample. A dispersion of SiC particles in the aluminum matrix is demonstrated after FSP, where some of the SiC particles have remained in their original size of 4.5 µm. It is also possible to discern the particle-matrix interface voids as shown by arrows in Figure 4.2. The introduction of second phase particles increased the refinement efficiency as the matrix grain size of the MMC was found to be slightly smaller. This was previously attributed to the Zener pinning effect of reinforcements [111].

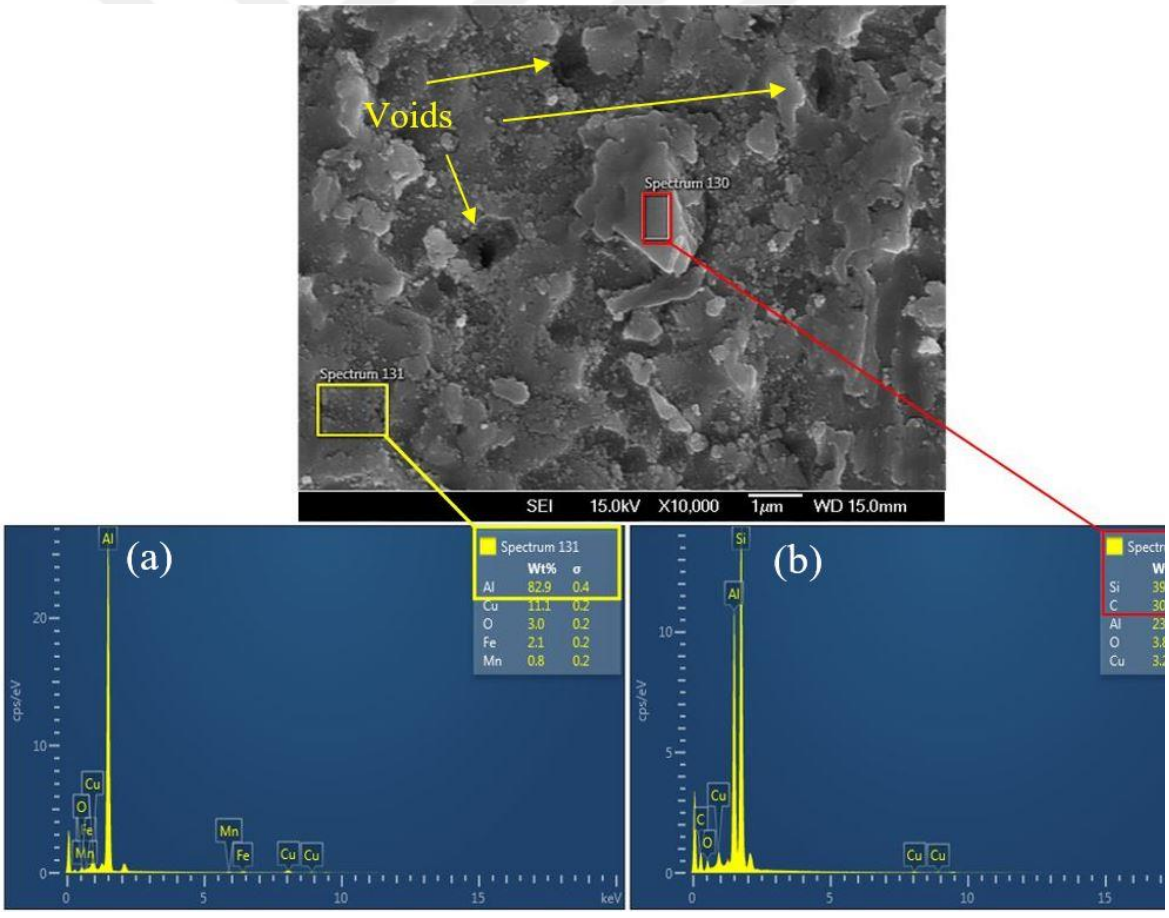

Figure 4.2 EDS analysis of the MMC sample from the (a) aluminum matrix and (b) SiC particle.

As shown in Figure 4.3, elemental mapping has been conducted on the MMC sample in order to observe the uniformity of SiC particles after 4 passes of back and forth processing. It can be seen that a bimodal distribution with the size range between 1.2 µm up to 4.5 µm of ceramic particles is achieved by fragmentation during FSP as attributed to the intense shearing applied by the tool that stirs the materials [112].

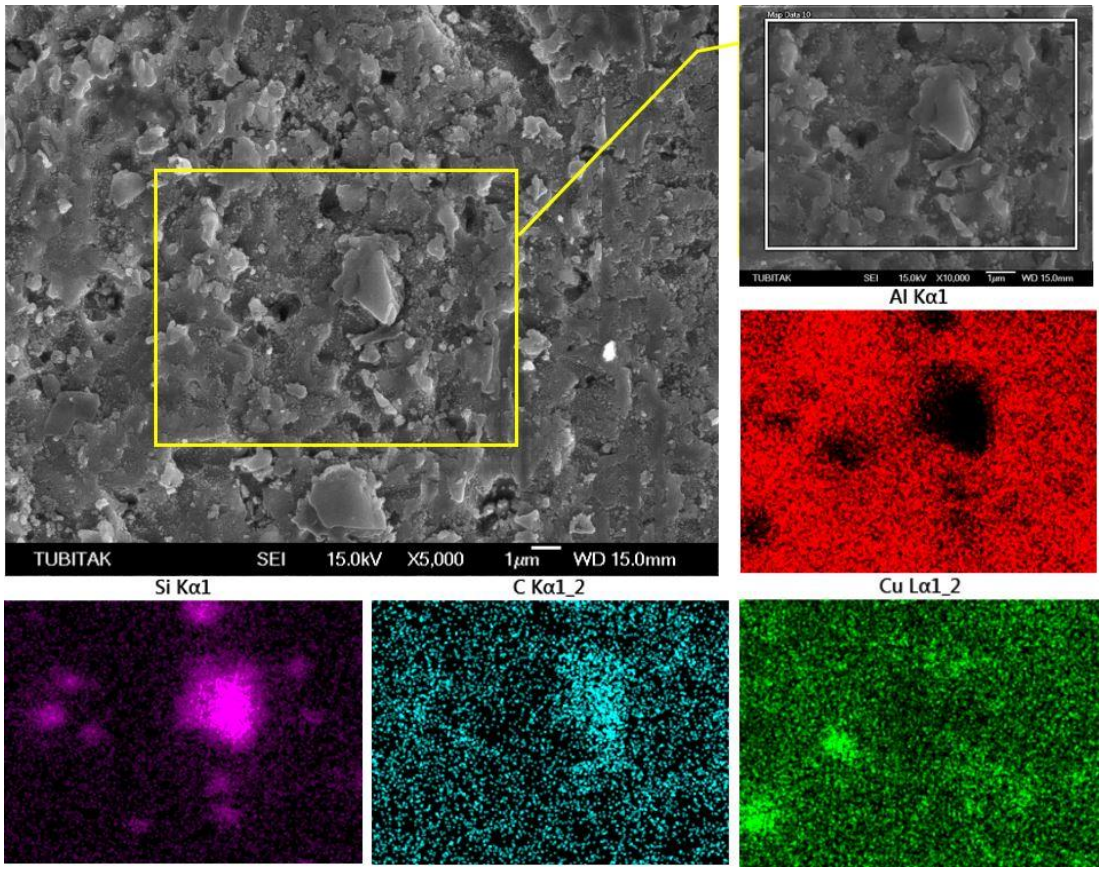

Figure 4.3 Elemental mapping of the MMC specimen

Figure 4.4 shows the microhardness measurements of Al2024 in as-received, FSPed and MMC conditions. The hardness profile depicts that the hardness of FSPed and MMC samples were improved up to 30% and 50% of the as-received condition, respectively. It can be followed from Fig. 4 that the hardness enhancement was observed on a wider zone when

changing the direction of passes during FSP. This is revealed by the delayed drop of hardness resulting in a symmetrical profile.

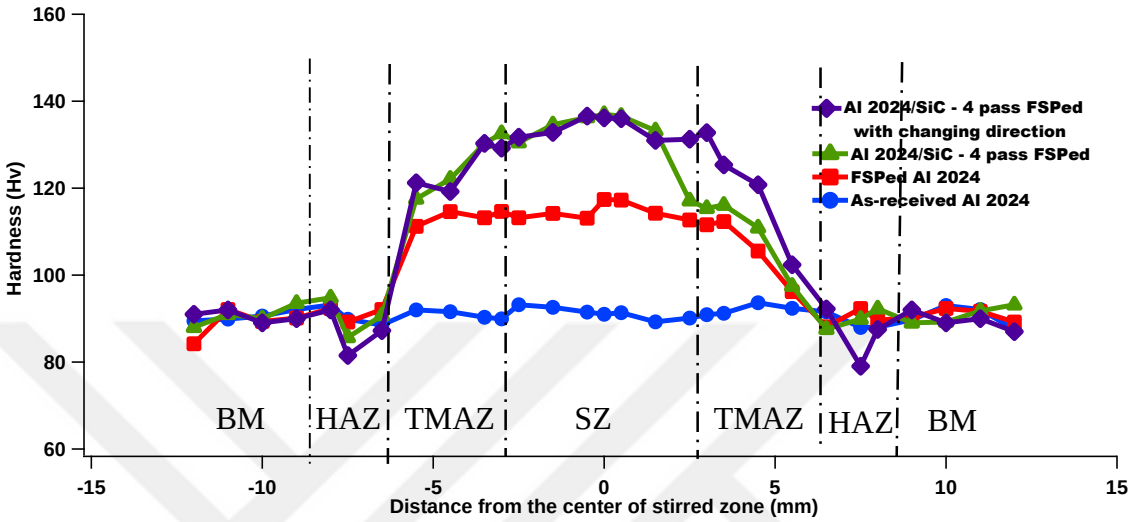

Figure 4.4 Microhardness of Al2024/SiC (MMC) tested from the cross-section of the plate.

4.2 Effect of temperature and strain rate on the mechanical behavior

This part describes the flow response of the as-received, FSPed and MMC conditions of Al2024 at room temperature and 300°C with the strain rates of 0.01, 0.001, 0.0001 s^{-1}. Figure 4.5 displays the true stress-strain curves of mentioned conditions at ambient temperature.

According to Figure 4.5a and b, FSP was able to enhance the yield strength of the as-received sample to about 2.5 folds, in relation with microstructural refinement. However, increase in the ultimate strength remained at 20%, due to loss of strain hardening capability.

At the same time, FSP reduced ductility down to about 4%, arising from obstructed dislocation motion. It can be followed from Figure 4.5c that in comparison to the FSPed sample, ceramic particles bring about a 20% improvement in the yield strength for the MMC sample in part due to a slightly smaller grain size. However, this observation can be primarily

linked to the Orowan strengthening mechanism due to dispersed particles along with the reduction of ductility [113-116].

Another topic of interest is the effect of strain rate on the deformation behavior as it has a direct influence on the utilization of a material in various rate-sensitive applications. It is fair to state that, generally aluminum alloys do not exhibit noticeable strain rate sensitivity at ambient temperature [117, 118]. This held true for all the microstructural conditions presented herein.

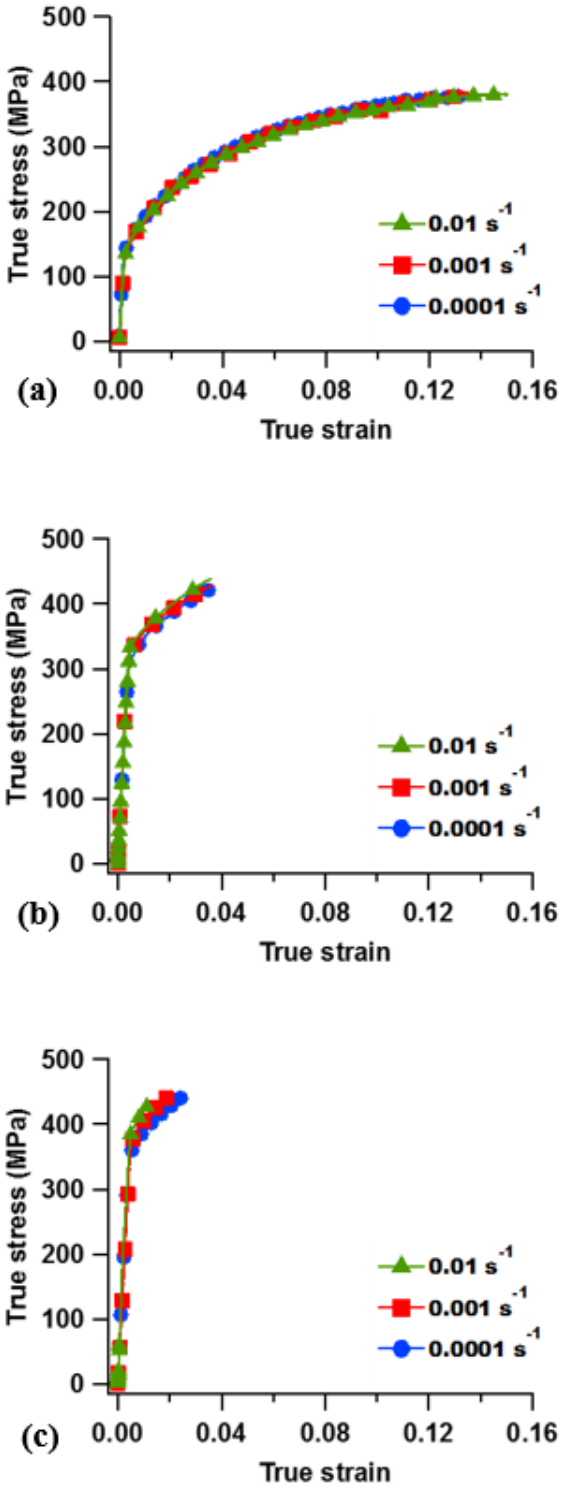

Figure 4.5 Room temperature flow curves of Al2024 (a) as-received; (b) FSPed; (c) Al2024/SiC MMC

In contrast, it is obvious that the flow stress levels are greatly influenced by the employed strain rate at elevated temperatures. The flow curves at 300°C for the as-received, FSPed and MMC conditions are shown in Figure 4.6 and it is revealed that there is a general tendency of rising flow stress levels with increase in the rate of straining.

This is especially important for the processed samples as can be imputed to their fine structure [119, 120]. It is worth noting that the improvement of flow stress levels is more significant for samples deformed at the highest strain rate. It is well-known that dynamic recrystallization (DRX) occurs at lower rates of deformation since the time required for energy accumulation and nucleation of newly recrystallized grains would be sufficient [121, 122]. Therefore, reduction in the flow stress enhancement can be associated with the occurrence of softening mechanisms such as DRX at lower strain rates.

It can also be observed that yield strength of FSPed samples increased up to 80 MPa and 120 MPa for the strain rates of 0.001 s^{-1} and 0.01 s^{-1}, respectively. Also comparing Figure 4.6b and Figure 4.6c, it can be understood that the level of strengthening was slightly lower for the MMC sample as could be associated with the reinforcement decohesion resulting in the growth of particle-matrix interface voids [47].

The Portevin-Le Chatelier (PLC) effect is manifested by serrated stress-strain curves, revealed at the higher strain rates employed in this investigation. PLC also named dynamic strain ageing (DSA) is typically attributed to dynamic interactions between gliding dislocations and mobile solute atoms leading to unstable plastic flow [123, 124]. Furthermore, the frequency of serrations has increased for FSPed and MMC samples, attributed to the grain refinement, consistent with the explanation that each serration relates to a yield point followed by a local Luders strain [125].

Also, elongations of the samples at all conditions have an improvement at highest strain rate. It is likely to relate this behavior to the dominating fracture mechanism being intergranular fracture under high strain rate and coalescence of voids at lower strain rates. This implies that cavitation played a significant role in the abrupt brittle failure [126, 127].

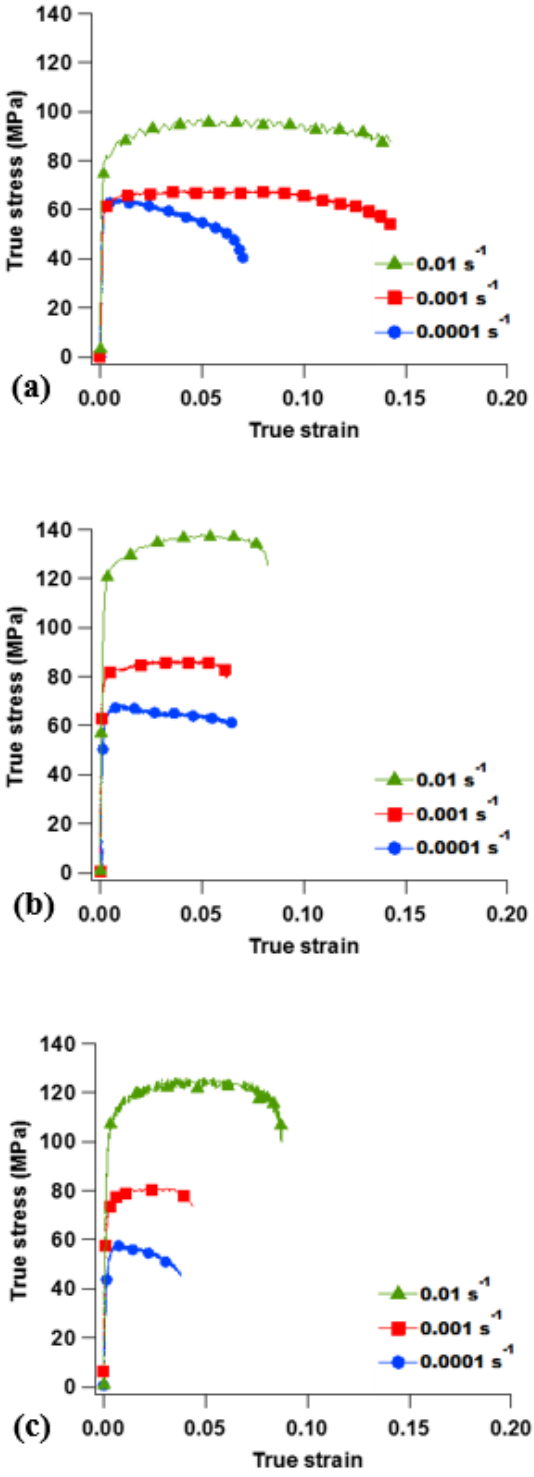

Figure 4.6 High temperature flow curves of Al2024 (a) as-received; (b) FSPed; (c) Al2024/SiC MMC at 300°C.

The strain rate sensitivity coefficient, *m* value can be calculated by the slope of $ln\,\sigma - ln\,\dot{\varepsilon}$ curve [128, 129].

$$m = \frac{\partial\, ln\,\sigma}{\partial\, ln\,\dot{\varepsilon}}\bigg|_{\varepsilon,T} \tag{2}$$

Figure 4.7 shows the variations of *m* value with true strain for different conditions. Contrary to the ambient temperature, strain rate sensitivity of all conditions at high temperature was significantly high. Also, *m* value for FSPed and MMC samples are two times higher than the as-received samples in conjunction with the different fracture mechanisms in the latter one, as explained further in the next section. Increased strain rate sensitivity is a typical phenomenon at high temperature as attributed to the grain boundary sliding (GBS) mechanisms aided by the refined grain structure [130]. In addition, *m* values exhibit an upward tendency with rising deformation strain.

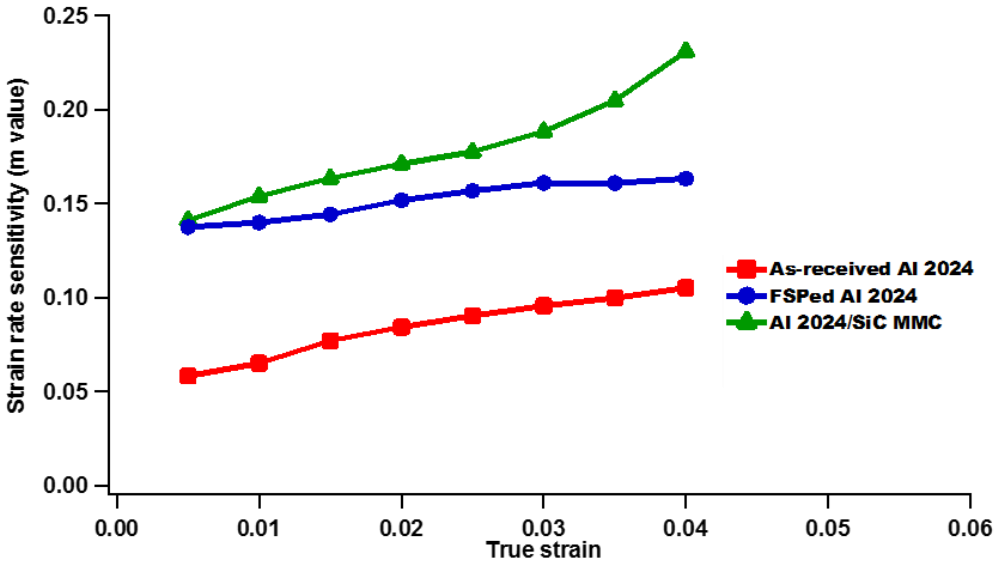

Figure 4.7 Effect of deformation strain on the strain rate sensitivity (*m*) value.

4.3 Fracture morphology analysis

In order to delineate the fracture mechanisms, further microscopy studies were employed for the as-received and processed samples at different temperatures and strain rates. Fracture morphologies of the samples are represented in Figure 4.8 Fracture surface under the strain rate of 0.01 s-1 tested at ambient temperature for (a) as-received Al2024; (b) FSPed Al2024; (c) Al2024/SiC; and tested at 300°C for (d) as-received Al2024; (e) FSPed Al2024; (f) Al2024/SiC MMC (Insets represent the low magnification images of each condition). both at ambient and high temperature (300°C), tested under the highest strain rate of $0.01s^{-1}$.

As shown in Figure 4.8a, a typical brittle failure consisting of a mixture of intergranular and cleavage features with a majority of the latter type, is clear for the as-received sample at ambient temperature. In contrast, at high temperature, the fracture surface includes a high density of serpentine sliding zones distributed on the inner wall of the dimples, and blade type edges on the dimple boundaries both of which could ensue by shearing of the dimple surfaces under a perpendicular principal stress [121].

Moreover, it can be asserted that the growth and coalescence of microvoids exacerbate the mechanical performance and affect the fracture behavior at the elevated temperature of 300°C. On the contrary, the type of fracture for the FSPed and MMC conditions is mostly intergranular and in brittle nature at room temperature. With the increase in deformation temperature, the FSPed sample still indicates a brittle fracture behavior, while the MMC sample exhibits a nucleation-controlled fracture mechanism with deeper void structure as a typical ductile feature. However, the brittle behavior of this condition could be ascribed to the variation of strength mismatch between the metal matrix and the ceramic

particles [131, 132]. Strength mismatch typically results in particle decohesion especially at high temperatures [133].

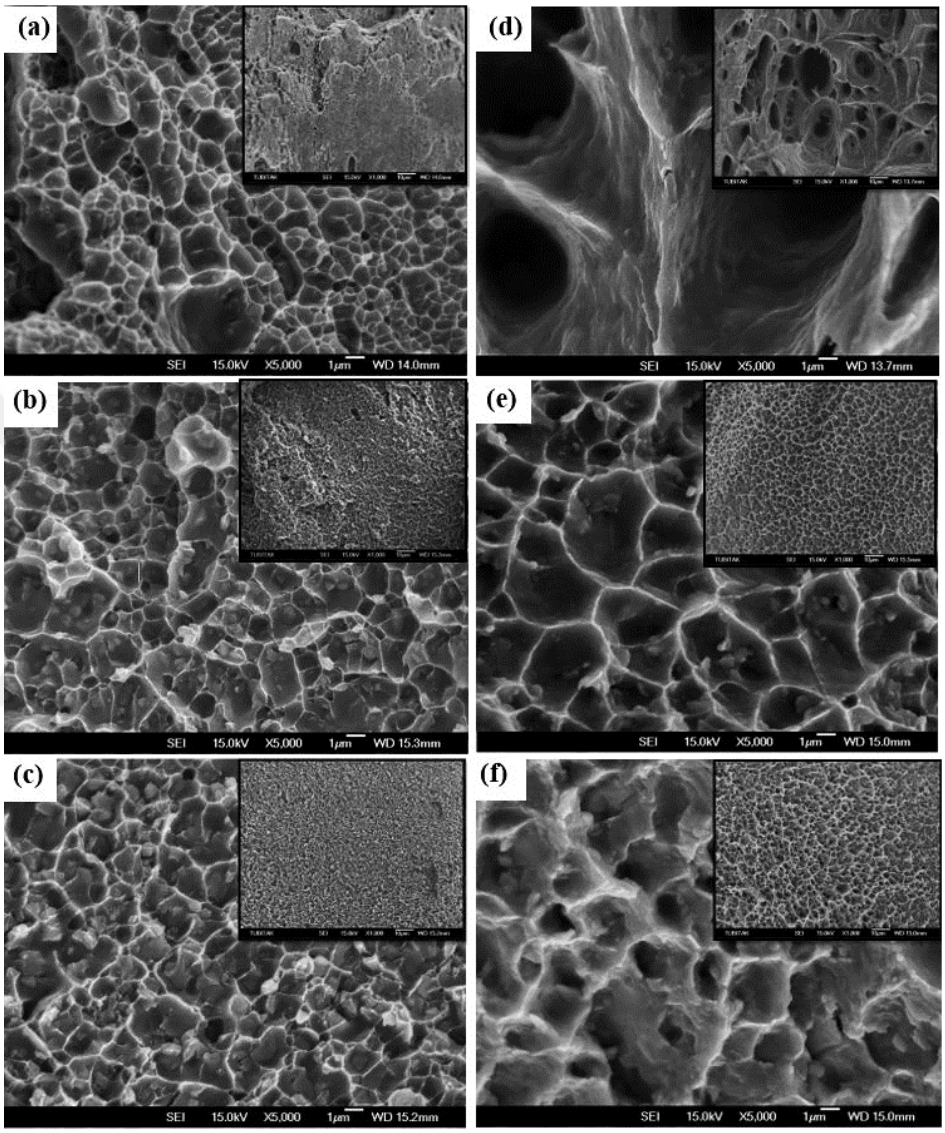

Figure 4.8 Fracture surface under the strain rate of 0.01 s^{-1} tested at ambient temperature for (a) as-received Al2024; (b) FSPed Al2024; (c) Al2024/SiC; and tested at 300°C for (d) as-received Al2024; (e) FSPed Al2024; (f) Al2024/SiC MMC (Insets represent the low magnification images of each condition).

Figure 4.9 represents a comprehensive view of the strain rate effect on the fracture mechanisms of FSPed and MMC samples at high temperature. As shown in the bottom row of Figure 4.9, the fracture surfaces of the Al2024/SiC MMC samples deformed at the highest strain rate are covered with a significant amount of fine voids and equiaxed dimples (Figure 4.9d).

With decreasing strain rate to $0.001s^{-1}$, the mode of fracture is still mainly intergranular without deep dimples leading to the abrupt failure and low ductility. Noteworthily, at the lowest strain rate, adequate duration provides an opportunity for the coalescence of voids and dimples resulting in deeper and larger formations. The same behavior of fracture can be seen in Figs. 9a-c for the FSPed samples tested under various strain rates.

In general, Figure 4.9 depicts that the void size of the MMC sample is finer than that of the FSPed condition at all strain rates, owing to the stabilizing effect of distributed SiC particles on the grain boundary mobility at high temperature [132]. Notwithstanding the SiC stabilizers, mechanical behavior of both MMC and FSPed samples are similar which could be related to the particle decohesion in the MMC sample [47].

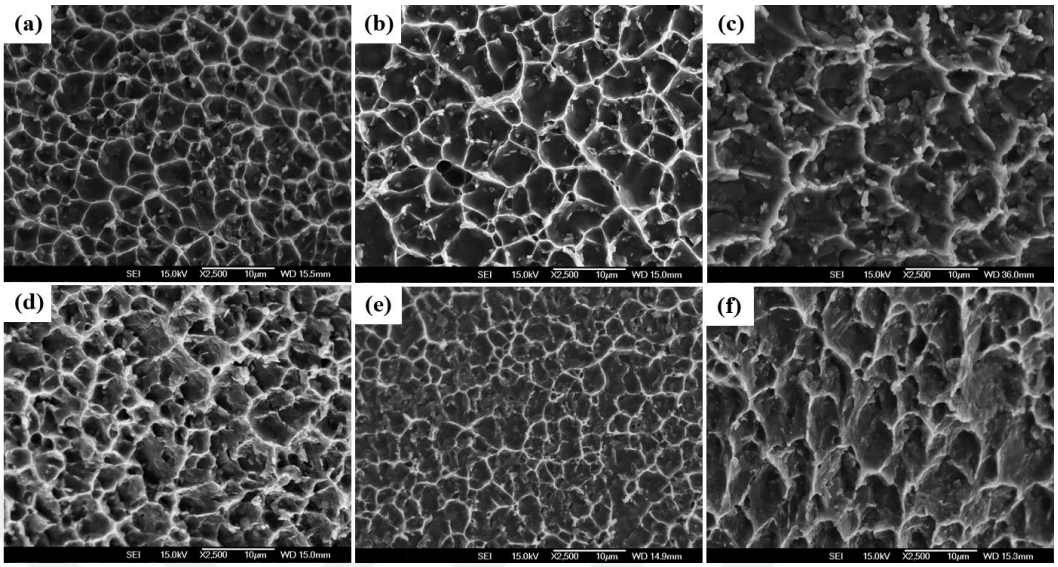

Figure 4.9 High temperature fracture surface of FSPed Al2024 tested under strain rate of (a) 0.01 s^{-1}, (b) 0.001 s^{-1} (c) 0.0001 s^{-1}; and Al2024/SiC MMC tested under strain rate of (d) 0.01 s^{-1}, (e) 0.001 s^{-1} and (f) 0.0001 s^{-1}.

4.4 Effect of FSP parameters on the mechanical behavior

From a structural point of view, high strength should be accompanied with decent ductility levels. As such, elongation values over 5% are generally preferred. In an attempt to identify the parameters yielding improved ductility, the response factor is re-identified. With the updated set of parameters including tool rotational speed of 1600 rpm, traverse speed of 30 mm/min and plunge depth of 0.2 mm, the effect on mechanical behavior is exhibited in Figure 4.10.

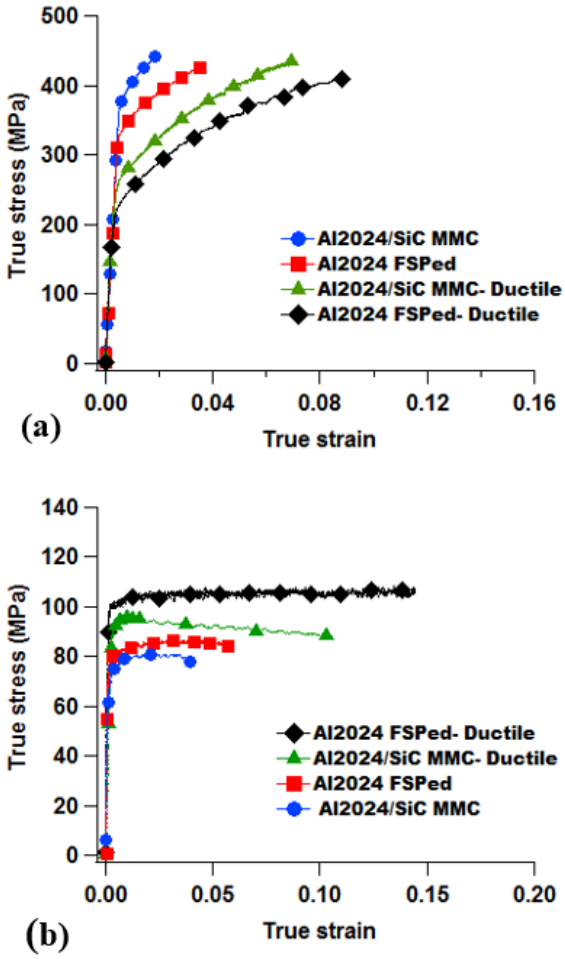

Figure 4.10 Effect of processing parameters on the (a) room temperature and (b) high temperature flow curves of Al2024 after friction stir

Accordingly, higher tensile strain levels are achieved for both the FSPed and MMC conditions, reaching up to 8 and 10%, respectively at ambient temperature. This enhancement can be connected to the elimination of porosities and voids with increased plunge depth [134]. Though it comes with the expense of lower strength due to the enlargement of stirred grains during lower traverse speed processing [135-137]. Increased temperature brings about an almost elastic perfectly plastic behavior after FSP. However, the MMC samples exhibited noticeable softening and thus could not surpass the ductility of the former which could be linked to particle decohesion at elevated temperatures [138, 139].

4.5 Summary on Al2024/SiC MMC fabricated by FSP

In this chapter, the effect of friction stir processing and the inclusion of SiC particles on the mechanical behavior of 2024 aluminum alloy at ambient and high temperatures were investigated. The effects of strain rate and deformation temperature on the fracture characteristics were discussed. The conclusions are drawn as follows:

1. Embedding SiC particles enhanced the microhardness of FSPed samples up to 50% relative to the as-received condition. This improvement is attributed to the grain refinement and uniform distribution of both large and fragmented SiC particles at the SZ.
2. The yield strength of as-received samples improved about 2.5 folds, in relation with the refined microstructure after FSP. SiC particles were effective in the further improvement of the yield strength of the MMC sample.
3. Adjustment of the processing parameters enabled the achievement of improved elongation levels reaching 10% and 15% at ambient and high temperature conditions, respectively.
4. The flow curves at high temperature were notably influenced by the deformation temperature and strain rate. All conditions were insensitive to strain rate at ambient temperature.
5. Fracture surface analysis at high temperature revealed that the mechanism at high strain rate is dominated by intergranular fracture for fine grained FSPed and MMC samples, while the as-received sample is generally fractured by coalescence of microvoids even under high strain rate.

5 HIGH TEMPERATURE CHARACTERISTICS OF AZ31/SiC METAL MATRIX COMPOSITE FABRICATED BY FRICTION STIR PROCESSING

5.1 Microstructure and hardness characterizations

As shown in Figure 5.1a, the boundary between stir zone reinforced by SiC particles and base metal is obvious. The perfect bonding without any defects observed between these two surfaces. Also the Figure 5.1b illustrates the uniformly distributed SiC particles inside of the matrix which is attributed to four pass FSP with rectangular shape pin of the FSP tool. Fragmented SiC particles are detected in Figure 5.1b, which are attributed to the cutting effect of the tool pin throughout the stirring process.

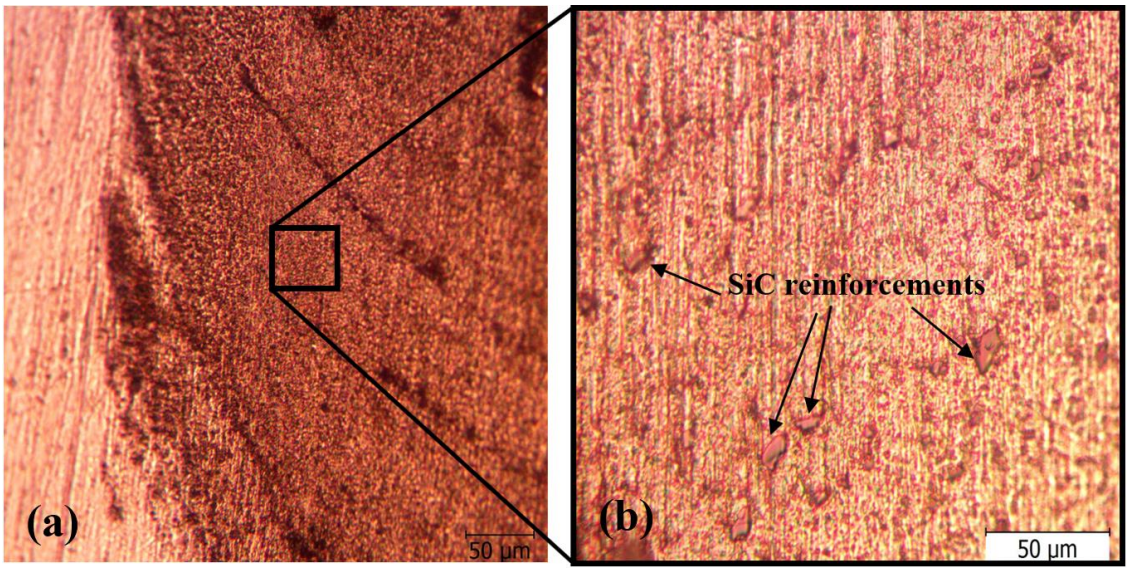

Figure 5.1 (a) Base metal and reinforced zone boundary (b) SiC reinforcements distribution.

In order to see the effect of temperature and strain rate on the microstructure of AZ31, samples were quenched in water. After mounting samples were ground and polished then observed in optical light microscope. As it is shown in Figure 5.2a, c and e the average grain size for the annealed, FSPed and AZ31/SiC MMC samples are decreased respectively. Based on the relationship between grain size and Zener–Holloman parameter, Chang et al. suggested the following equation to estimate the microhardness of AZ31 [140]:

$$Hv = 40 + 72\, d^{-0.5} \quad (3)$$

where d is the mean grain size of the AZ31 magnesium alloy. According to the mentioned equation and the grain size of different conditions, the microhardness of samples are estimated and written in Table 5.1. These values revealed an acceptable agreement with the experimental results as shown in Table 5.1. Nevertheless, the average microhardness of the AZ31/SiC MMC at stir zone was about 87 which is higher than the estimated value. It is considered that this difference was reflected by not only the grain refinement but also the pinning effect of hard SiC ceramic particles.

Table 5.1 Grain size and microhardness value of AZ31 at different conditions.

Sample	Mean grain size (μm)	Estimated hardness (Hv)	Actual hardness (Hv)
Annealed AZ31	52	49.98	48
FSPed AZ31	13	59.97	66
AZ31/SiC	5	72.20	87

Figure 5.2a, b show the microstructure of the annealed AZ31 tested at room and high temperature under the constant strain rate of 0.001 s^{-1}. Comparing these two microstructures, it can be found that the nucleation of new grains and recrystallization were started and grain growth occurred during the high temperature tensile test. Approximately the same scenario is happened for the FSPed and MMC samples but with a big difference in magnitude and the grain growth in annealed sample was considerably greater than the other conditions.

Also Figure 5.2 shows that the effect of temperature on the FSPed samples is more considerable than the MMC. Grain growth was confirmed at 300˚C for the FSPed sample without the SiC particle may be because of the residual strain received by the FSP. On the contrary, the grain size was nearly the same for the AZ31/SiC MMC samples even after high temperature tensile test under the strain rate of 0.001 s^{-1}, attributed to the pinning effect of the SiC particles located on the grain boundaries.

In order to see the effect of heating duration through the tests, microstructures of fractured samples tested at different strain rates are shown in Figure 5.3. The results are confirmed that decreasing the strain rate for all conditions caused the nucleation of new grains mostly under the strain rate of 0.001 s^{-1} and grain growth of the samples at lowest strain rate (Figure 5.3). But the nucleation and grain growth in the FSPed samples were more than those of MMC in relation with the suppression of the dynamic grain growth and recrystallization by SiC particles. All microstructures were recorded from the unstrained regions of the samples.

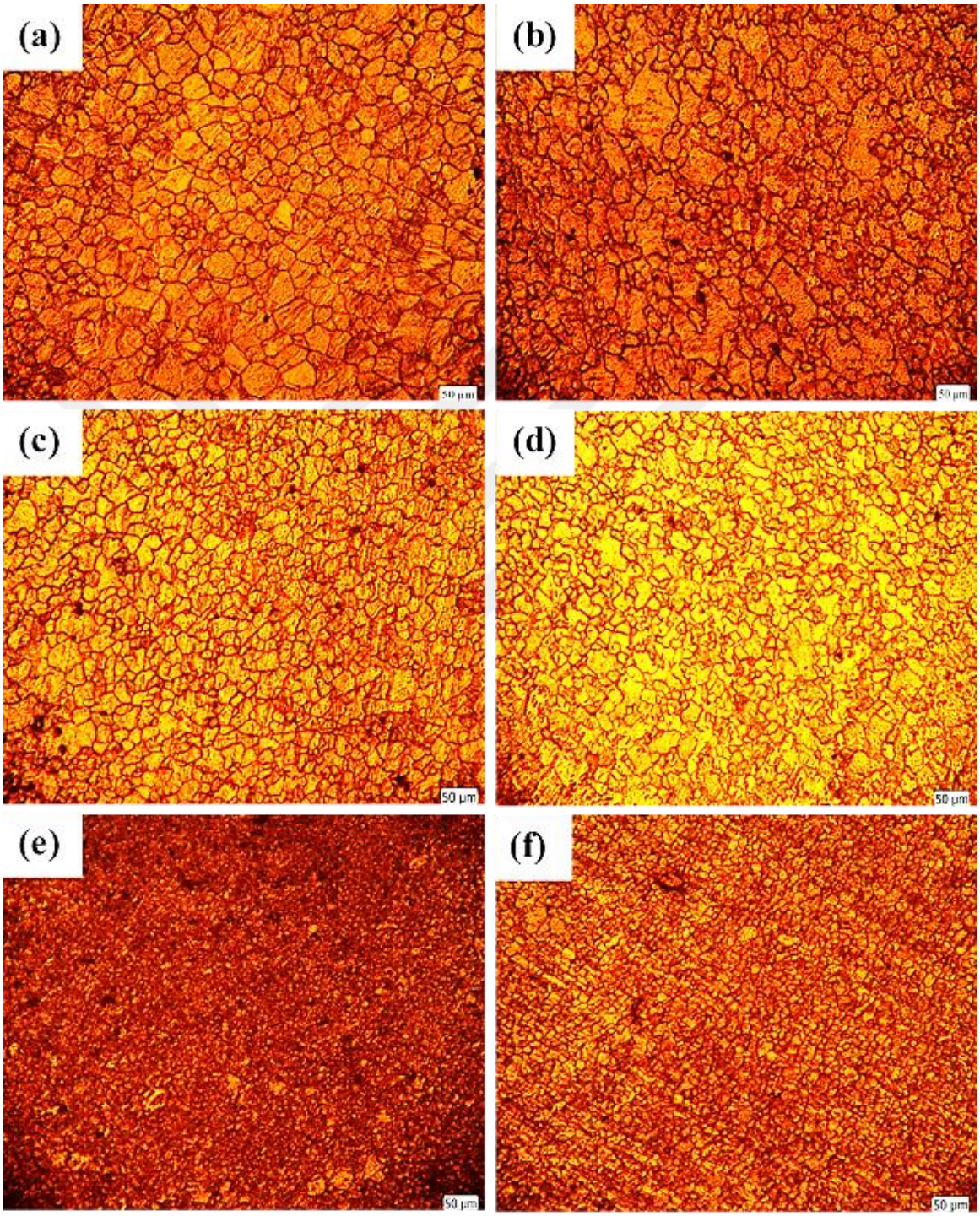

Figure 5.2 Microstructure of AZ31 (a) annealed, (c) FSPed, (e) MMC after tensile test at room temperature and (b) annealed, (d) FSPed and (f) MMC after tensile test at 300˚C under the strain rate of 0.001 s^{-1} (all images were recorded at the magnification of 20x).

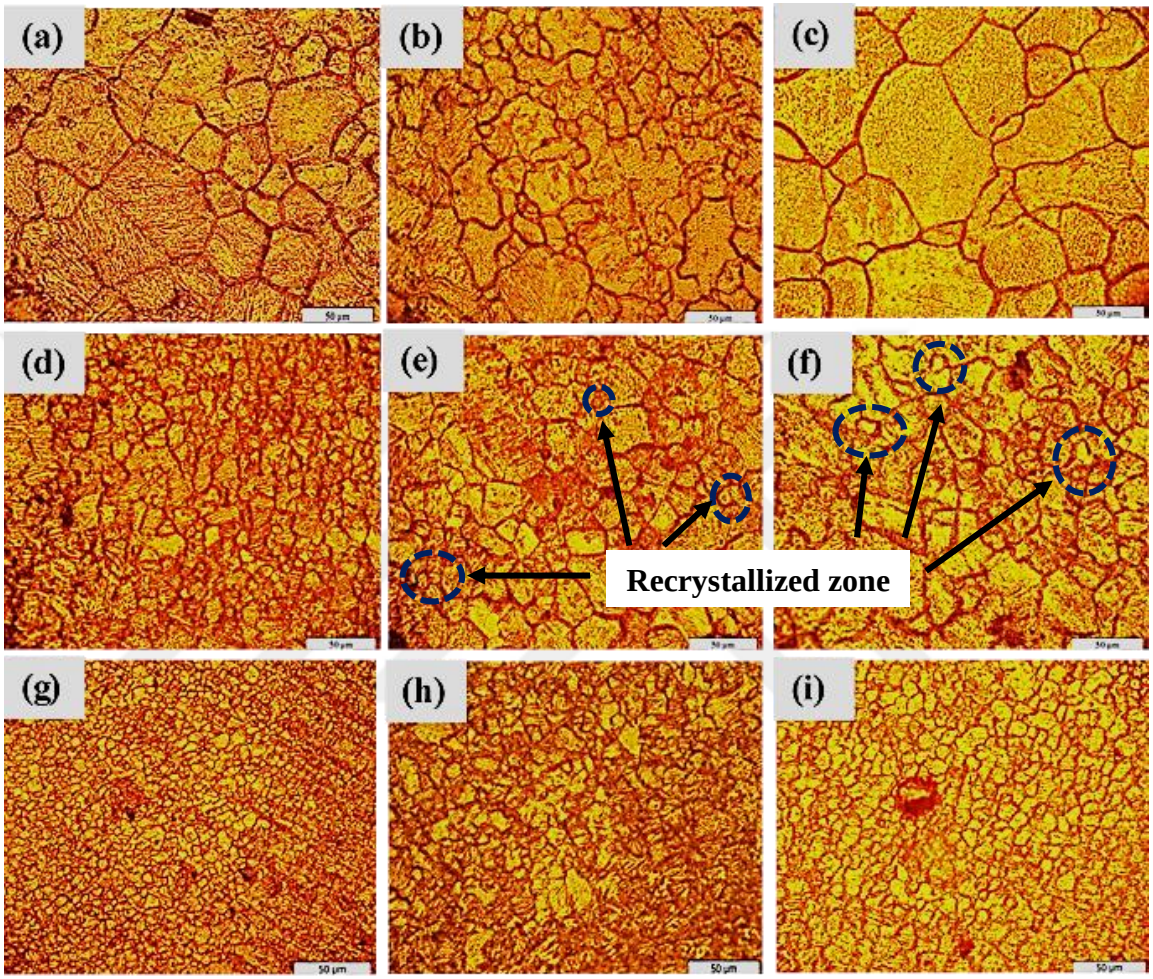

Figure 5.3 Microstructure of AZ31 after the tensile test at 300˚C for annealed under strain rate of (a) 0.01 s^{-1}, (b) 0.001 s^{-1}, (c) 0.0001 s^{-1}, FSPed under the strain rate of (d) 0.01 s^{-1}, (e) 0.001 s^{-1}, (f) 0.0001 s^{-1} and AZ31/SiC MMC under the strain rate of (g) 0.01 s^{-1}, (h) 0.001 s^{-1}, (i) 0.0001 s^{-1} (all images were recorded at the magnification of 50x).

The results of microhardness tests are demonstrated in Figure 5.4. The enhancements of the hardness after the FSP is obvious for both FSPed and MMC conditions as compared with the annealed sample. A reduction of hardness is observed at both advancing and retreating sides of stir zone which is named heat affected zone attributed to the grain growth

at this part caused by the heating throughout the FSP. 30% for FSPed and about 80% improvement in microhardness for MMC samples were achieved after the process.

By comparing the hardness profiles of FSPed and MMC samples, it can be understood that the hardness of FSPed samples is more stable than that of MMC. This may be attributed to the effect of the hardness of SiC particles individually at certain regions.

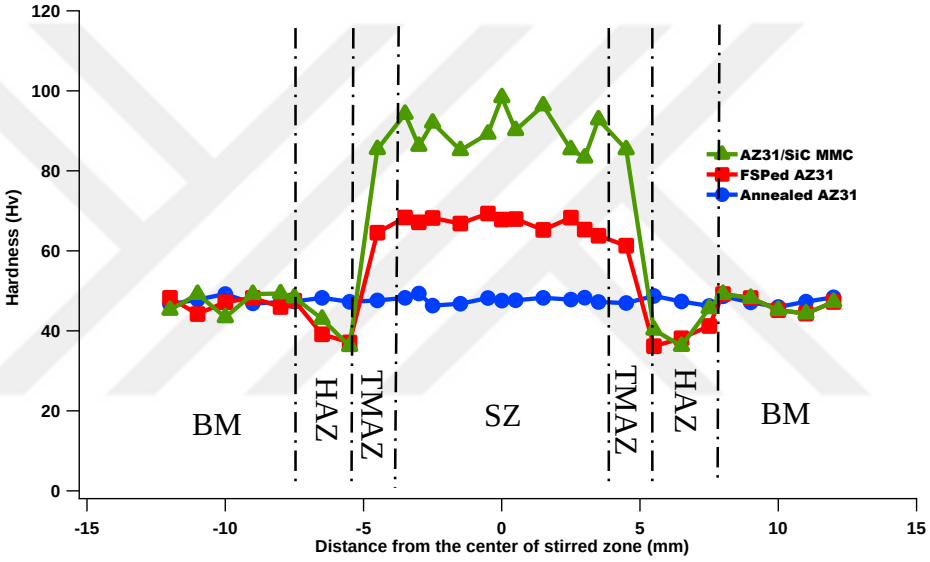

Figure 5.4 Microhardness of annealed AZ31, FSPed and AZ31/SiC MMC tested from the cross-section of the plates.

5.2 Effect of temperature and strain rate on the mechanical behavior

The flow tensile behavior of the as-received, FSPed and MMC conditions of AZ31 at ambient temperature and 300˚C at different strain rates of 0.01, 0.001, 0.0001s^{-1} was discussed in this section. Figure 5.5 demonstrates the true stress-strain curves of aforementioned conditions at ambient temperature.

The restricted number of slip systems, and consequently the limited ductility in hcp metals like magnesium alloys may need FSP to accommodate severe plastic deformation by activating non-basal slip systems. Comparing the Figure 5.5a and b reveals that friction stir processing has improved the maximum true strain of the annealed sample, from 12% up to about 26%. Also the true stress-true strain curves of the samples indicate that the annealed AZ31exhibited the yield strength of around 120 MPa and FSP softened the material resulting the less yield strength of 80 MPa. These results are in a harsh contrast to the case when grain size is decreased by FSP.

The reduction in strength and rise in tensile elongation after SPD process agree well with the reports by Mukai et al. about the ECAP of AZ31 [141]. Limited ductility in hcp metals like magnesium alloys in relation with restricted number of slip systems, can be improved by FSP. This enhancement comes from disintegration of AZ31 texture from a strong basal texture to the combination of basal and non-basal slip systems like prismatic texture because of the severe plastic deformation at high temperature during the FSP and the same behavior was reported by Kim et al. for AZ61 after high temperature ECAP and verified by pole figure analysis [142]. The similar texture transformation of magnesium alloys are observed during different methods of SPD [141, 143].

However, the UTS of the material is improved after the process and it means FSP enhances the formability of AZ31 and makes it a ductile, strain hardenable and formable material even at room temperature. This is in agreement with the results related in literatures [87, 144-146]. On the other hand, the addition of SiC to the AZ31 matrix has increased the

yield strength of FSPed samples, in relation with the Orowan strengthening mechanism due to reinforcements with expense of the reduction in ductility [114, 116].

Also it seems that the brittle fracture due to interaction between SiC hard particles and AZ31 soft matrix during the strain hardening part of tensile tests has important role in decreasing the ductility of MMC samples (Figure 5.5c). Also with looking at the results of the tensile tests at different strain rates, it can be concluded that all conditions are approximately insensitive to the strain rate at ambient temperature.

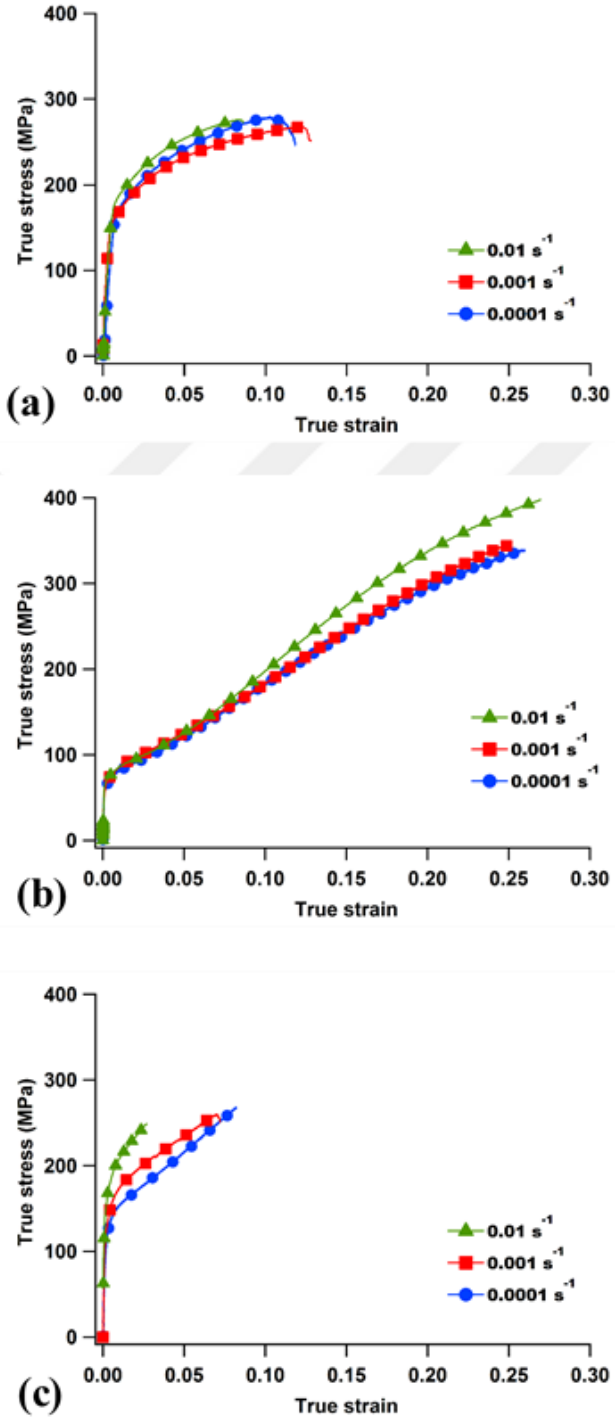

Figure 5.5 Ambient temperature flow curves of AZ31 (a) annealed; (b) FSPed; (c) AZ31/SiC MMC.

The true stress versus true strain curves of the annealed AZ31, FSPed and AZ31/SiC MMC are shown in Figure 5.6 for various strain rates at high temperature of 300˚C. Unlike the ambient temperature, high temperature flow curves illustrate that the flow stress levels are significantly affected by the tensile strain rate. For all conditions the flow stress level of high strain rate of 0.01 is greater than the others, in relation with the formation of tangled dislocation arrangements, as obstacles to dislocation movement, due to the higher strain rates [147].

With comparing the Figure 5.5 and Figure 5.6 it is revealed that flow stress level of all conditions has a significant reduction at high temperature. The activation of different slip systems of hcp structure and also decreasing the hindering effect of twins at high temperature is considered to be the key reason for the observed behavior [147]. Also considering the Figure 5.5b and c, the flow stress level both FSPed and MMC samples are relatively lower than the annealed AZ31 linked to the transformation of texture and orientation of grains throughout the SPD process [143].

The true stress–true strain curves of FSPed condition tested under strain rates of 0.001 s^{-1} and 0.0001 s^{-1} demonstrate a flow behavior including a peak stress at certain strain, after which the flow stresses drop monotonically down to the steady state level which is attributed to the happening of dynamic recrystallization (DRX) as major restoration mechanism during high temperature deformation at low strain rates [148]. This can also be proved by the microstructural observation after high temperature testing, the samples which are shown in Figure 5.3e and f.

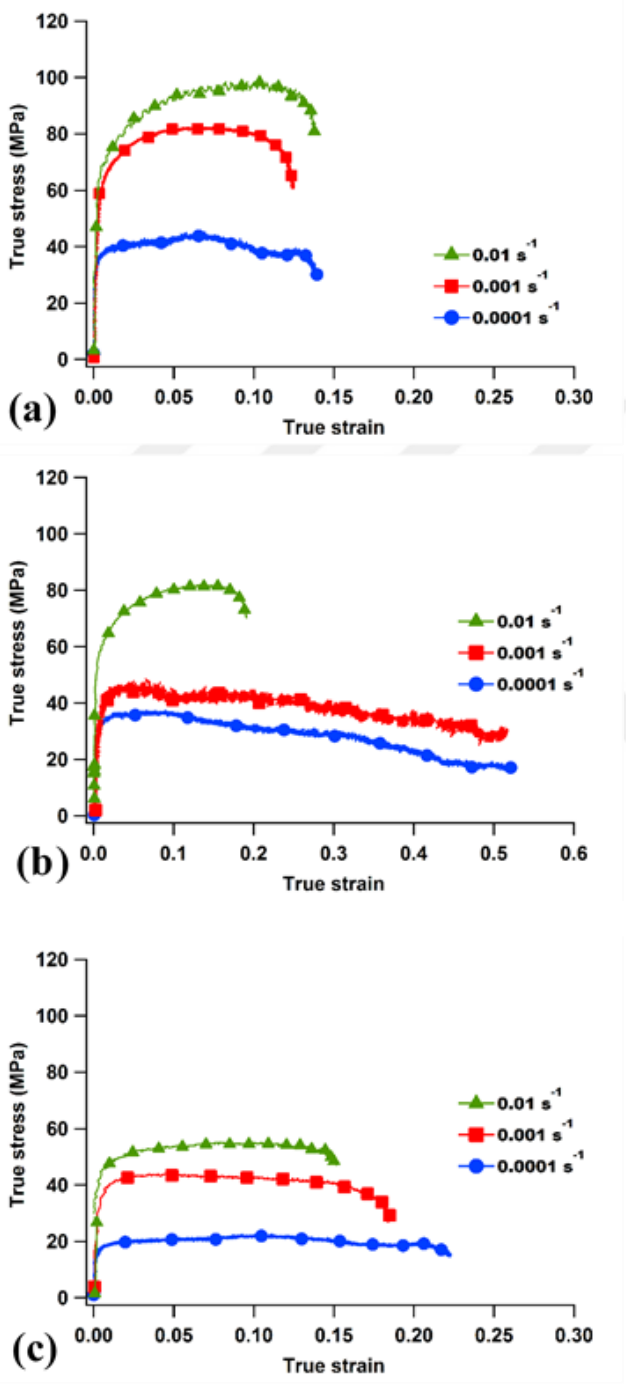

Figure 5.6 High temperature flow curves of AZ31 (a) annealed; (b) FSPed; (c) AZ31/SiC MMC at 300˚C.

The strain rate sensitivity coefficient (*m* value) of AZ31 for all conditions is calculated by the slope of $\ln \sigma - ln\, \dot{\varepsilon}$ curve , as it was previously calculated for Al2024 [128, 129].

$$m = \frac{\partial\, ln\, \sigma}{\partial\, ln\, \dot{\varepsilon}}\Big|_{\varepsilon,T} \tag{2}$$

As oppose to the ambient temperature, strain rate sensitivity of all conditions at high temperature was noticeably larger around 0.20. Strain rate sensitivity of annealed and FSPed samples revealed an upward tendency with increasing tensile strain because of the recrystallization and grain growth taking place in samples tested at low and intermediate strain rates. On the other hand, MMC samples exhibit a relatively constant trend of *m* value of 0.21, in relation with stable microstructure at different strain rates which is evidenced in Figure 5.4g, h and i.

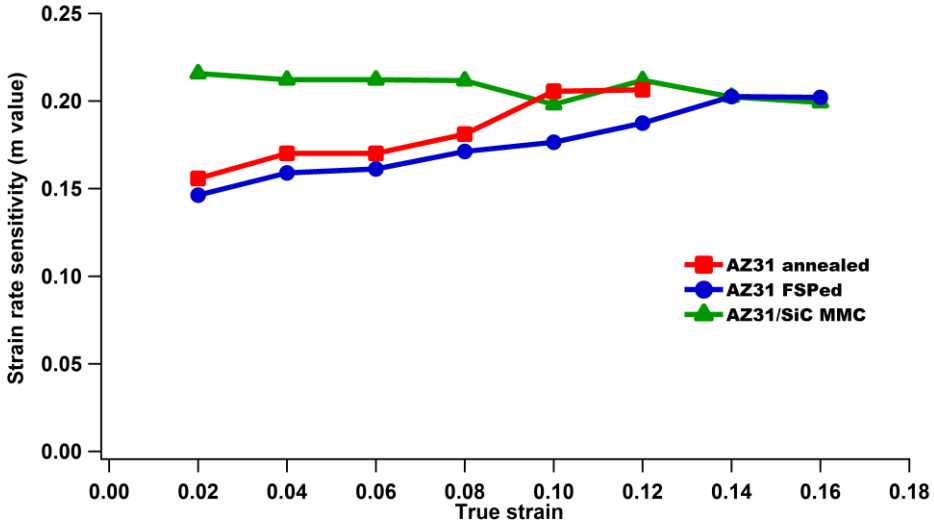

Figure 5.7 Effect of deformation strain on the strain rate sensitivity (m) value.

5.3 Fracture morphology analysis

In order to observe the fracture mechanism of tested samples, further SEM analysis was employed for the fracture surfaces of the samples, tested at different temperature and strain rates. Fracture morphologies of the specimens are represented in Figure 5.8 both at ambient and high temperature of 300 ˚C, tested under the intermediate strain rate of 0.001 s^{-1} to observe the effect of temperature on the fracture mechanism of each condition. At room temperature the annealed displayed limited ductility with fracture in tension and the observations revealed locally brittle mechanisms of fracture (Figure 5.8a).

Contrary to room temperature, major fracture mechanism of annealed AZ31 is ductile fracture with coalescence of voids and ductility of samples were limited by failure of dimples occurring on the coarse grains at high temperature (Figure 5.8d). Figure 5.8b illustrates the surface of FSPed sample covered by fine voids and equiaxed dimples refer to the completely difference between texture of FSPed and annealed condition which is discussed in previous sections. Also, deep dimples of FSPed sample at high temperature indicate the typical ductile fracture which is sharply in agreement with the flow tensile tests result (Figure 5.6). The main fracture mechanism of AZ31/SiC MMC at high temperature is a mixture of brittle fracture caused by interaction between hard SiC particles and soft magnesium matrix with big dimples made by fast fracture behavior at room temperature. However, at high temperature coalescence of the voids and also particle decohesion of clustered ceramic reinforcements at the grain boundaries are the most effective fracture mechanisms (Figure 5.8f).

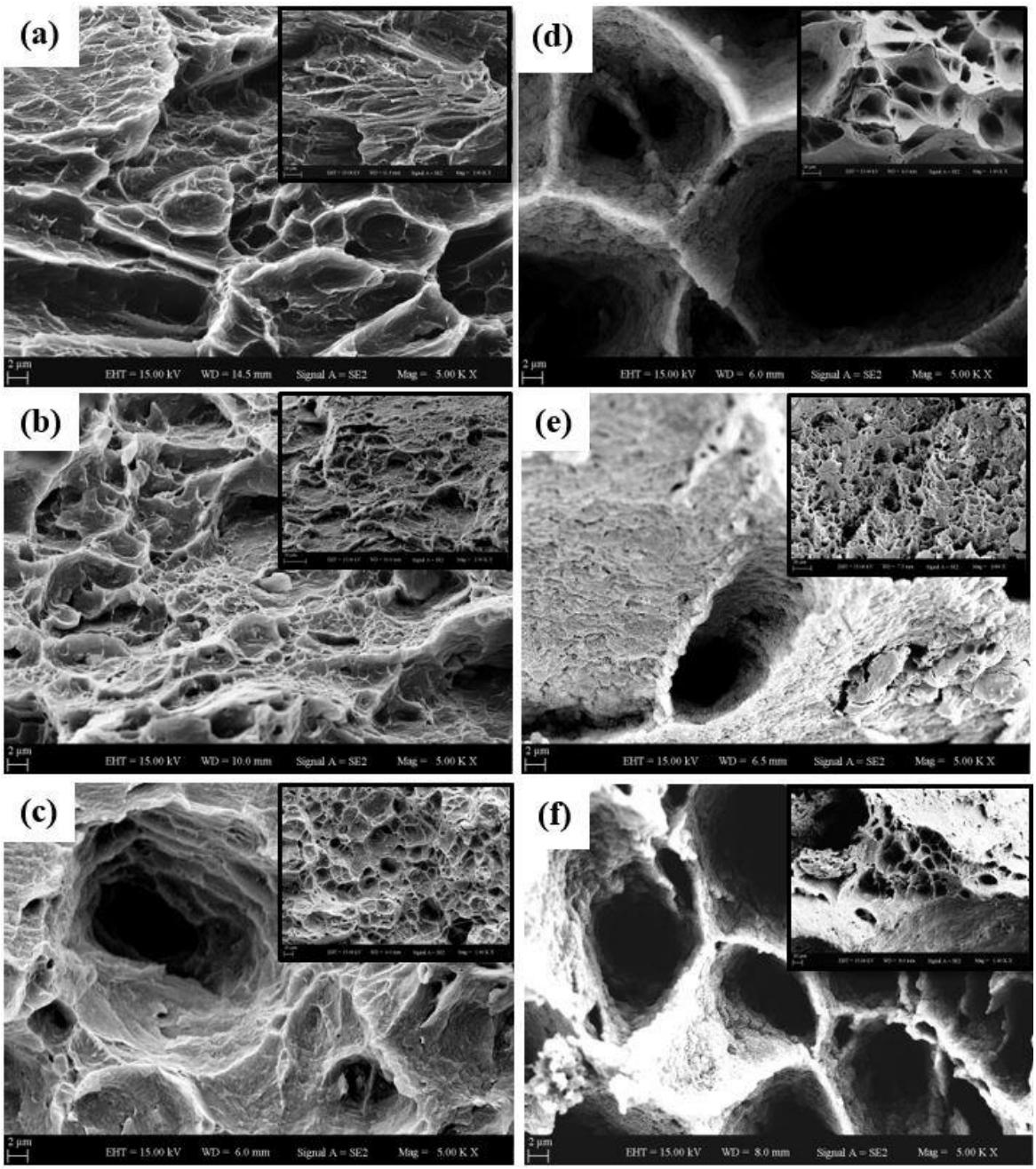

Figure 5.8 Fracture surface under strain rate of 0.001 s^{-1} tested at ambient temperature for (a) Annealed AZ31 ; (b) FSPed AZ31; (c) AZ31/SiC; and tested at 300°C for (d) Annealed AZ31; (e) FSPed AZ31; (f) AZ31/SiC MMC (Insets represent the low magnification images of each condition).

Figure 5.9 prepared with the purpose of studying the influence of strain rate on the fracture mechanisms of FSPed and MMC samples at high temperature. As shown in left side of Figure 5.9 the fracture surfaces of FSPed samples are covered with equiaxed and deep dimples for all strain rates. However, with decreasing the strain rate from 0.01 s^{-1} to 0.0001 s^{-1} the number of dimples are increased and the sine of them are decreased attributed to the recrystallization of new grains which was observed in microstructure of FSPed samples (Figure 5.3).

On the other hand, relatively brittle manner of fracture mechanism of AZ31/SiC MMC sample tested at high strain rate of 0.01 s^{-1} is observed in Figure 5.9d and clustered SiC particles easily are displayed at high magnification SEM image. Although, the deeper dimples related to the ductile fracture behavior can be seen for lower strain rates, still the major fracture were happened because of particle decohesion of SiC reinforcements which is explained at previous chapter.

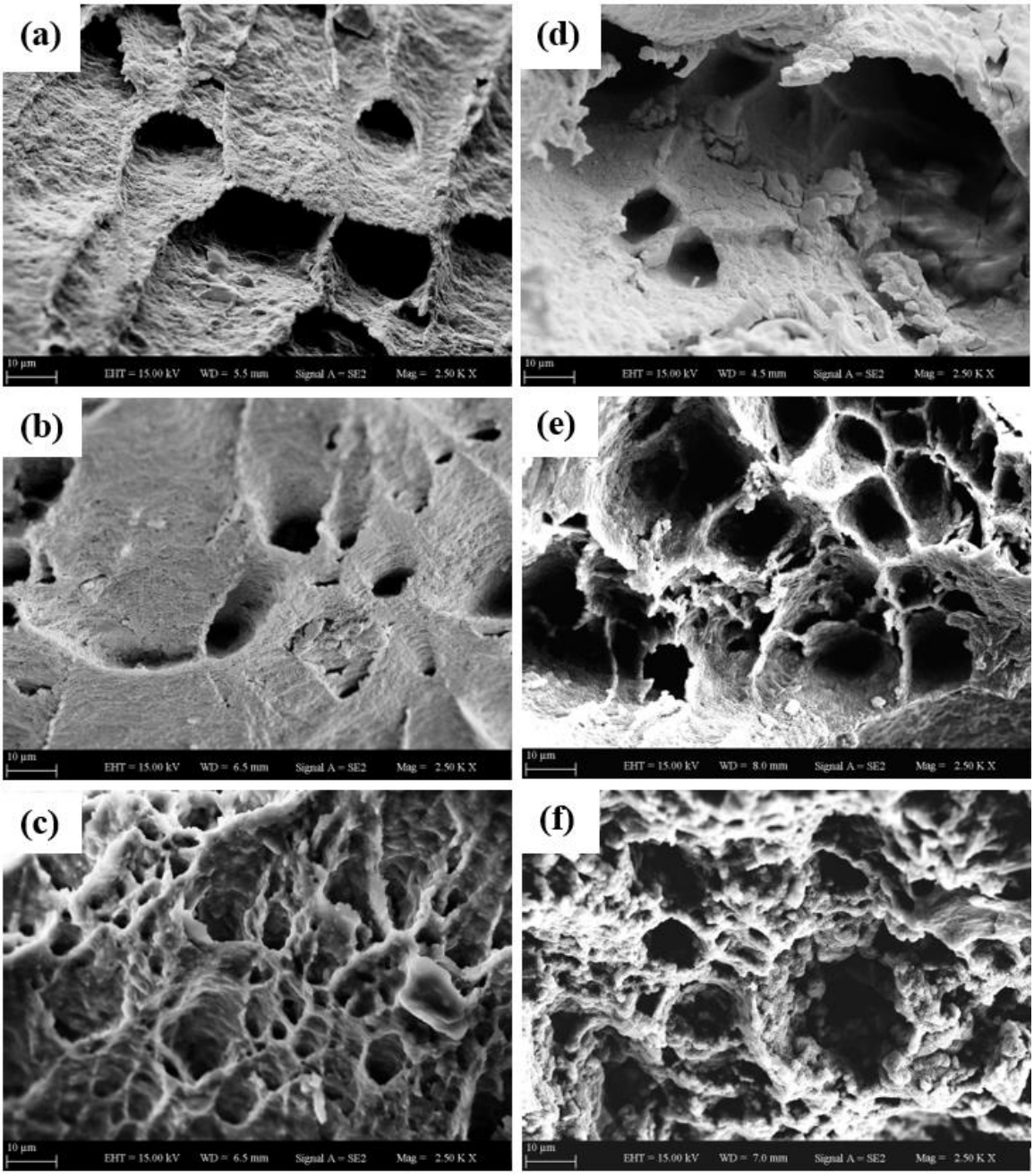

Figure 5.9 High temperature fracture surface of FSPed AZ31 tested under strain rate of (a) $0.01s^{-1}$, (b) $0.001s^{-1}$ (c) $0.0001s^{-1}$; and AZ31/SiC MMC tested under strain rate of (d) $0.01s^{-1}$, (e) $0.001s^{-1}$ and (f) $0.0001s^{-1}$.

5.4 Summary on AZ31/SiC MMC fabricated by FSP

In this chapter, the influence of friction stir processing and embedding the SiC particles on the mechanical behavior of AZ31 magnesium alloy at ambient and high temperatures were studied. The effects of deformation temperature and strain rate on the microstructure and fracture mechanisms of different conditions were discussed. The conclusions were drawn as follows:

1. Friction stir processing was successfully applied on the AZ31 in order to fabricate the AZ31/SiC MMC and perfect bonding without any defects observed between base metal and reinforced zone.

2. Ductility values for the FSPed samples are markedly higher than that of the annealed alloy at both high temperature and room temperature under various strain rates, indicating that the formability of FSPed AZ31 was increased at room temperature.

3. Inclusion of SiC particles improved the microhardness of FSPed samples up to 80% relative to the annealed condition, in relation with the grain refinement and uniform distribution SiC particles.

4. The flow curves at high temperature were notably influenced by the deformation temperature and strain rate. All conditions were insensitive to strain rate at ambient temperature.

5. Fracture surface analysis at ambient temperature revealed the ductile fracture of fine grained FSPed samples represented by equiaxed and relatively deep micro voids, while the annealed and MMC samples demonstrated a relatively brittle fracture.

6 CONCLUSION

This thesis is motivated by the promptly increasing interests in the development of friction stir processing (FSP) of light alloys and fabrication of metal matrix composites (MMCs) and a lack of fundamental knowledge of high temperature behavior of these materials. Several experiments were conducted to achieve defect free FSPed and uniform particle dispersion in MMCs of aluminum and magnesium alloys. The mechanical properties of processed materials were observed at both ambient and high temperatures.

The results of microhardness tests show a significant enhancement after FSP in relation with the grain refinement and also distribution of SiC particles inside of the metal matrix for MMC samples. The yield and ultimate tensile strength of as-received Al2024 improves after FSP attributed to the grain boundary strengthening and Orowan strengthening with the expense of decreasing the elongation to failure. Fracture surface analysis at high temperature reveals that the mechanism at high strain rate is dominated by intergranular fracture for fine grained FSPed and MMC samples, while the as-received sample is generally fractures by coalescence of microvoids even under high strain rate.

On the other hand, addition of SiC reinforcements improves the microhardness of FSPed samples up to 80% relative to the annealed AZ31. Also FSP declines the yield strength of AZ31 along with sharp improvement of ductility up to the maximum true strain of 26% at ambient temperature. The flow curves at high temperature are remarkably influenced by the deformation temperature and strain rate. Ductile fracture mechanism of fine grained FSPed samples of AZ31 characterized by equiaxed and relatively deep micro voids, while the annealed and MMC samples demonstrated a relatively brittle fracture.

Table 6.1 represents the effect of FSP on the mechanical properties of each condition.

Table 6.1 Effects of FSP on the mechanical properties and fracture behavior of Al and Mg light alloys.

Mechanical properties	FSPed Al2024	Al2024/SiC MMC	FSPed AZ31	AZ31/SiC MMC
Grain size (μm)	4.2	2.3	13	5
Hardness (Hv)	115	135	66	87
Yield strength (MPa)	320	380	70	120
Ultimate Tensile Strength (MPa)	410	390	330	240
Elongation at Failure (%)	4	3	26	8
High temperature flow strain (%)	14	11	52	21
Strain Rate Sensitivity	0.15	0.15-0.22	0.15-0.21	0.21
Fracture behavior at ambient conditions	intergranular brittle fracture	Brittle with decomposed SiC particles	Ductile with microvoids	Brittle with decomposed SiC particles
Fracture behavior at high temperatures	Intergranular brittle fracture	Ductile fracture with deep voids	Ductile with deep dimples	Coalescence of voids and particle decohesion

FUTURE WORKS

Although some efforts were made to investigate the mechanical behavior of friction stir processed and metal matrix composites of light alloys fabricated by FSP in the current study, these methods are not limited to the performed experiments and achieved results. Therefore, few suggestions for upcoming research efforts are listed below:

1. Ductility improvement of MMC samples can be achieved using different process parameters by changing the response factor of UTS with maximum strain.
2. The effect of post heat treatment can be observed in order to enhance the mechanical properties of the processed samples.
3. Response to various loading conditions is another aspect to be investigated.

BIBLIOGRAPHY

[1] Rao VK, Taplin D, Rao PR. The grain size dependence of flow and fracture in a Cr-Mn-N austenitic steel from 300 to 1300K. Metallurgical Transactions A. 1975;6:77-86.

[2] Lasalmonie A, Strudel JL. Influence of grain size on the mechanical behaviour of some high strength materials. Journal of Materials Science. 1986;21:1837-52.

[3] Hall E. The deformation and ageing of mild steel: III discussion of results. Proceedings of the Physical Society Section B. 1951;64:747.

[4] Petch NJ. The cleavage strengh of polycrystals. J of the Iron and Steel Inst. 1953;174:25-8.

[5] Armstrong R, Codd I, Douthwaite RM, Petch NJ. The plastic deformation of polycrystalline aggregates. The Philosophical Magazine: A Journal of Theoretical Experimental and Applied Physics. 1962;7:45-58.

[6] Armstrong RW. The influence of polycrystal grain size on several mechanical properties of materials. Metallurgical and Materials Transactions B. 1970;1:1169-76.

[7] Valiev RZ, Islamgaliev RK, Alexandrov IV. Bulk nanostructured materials from severe plastic deformation. Progress in Materials Science. 2000;45:103-89.

[8] Rosochowski A, Olejnik L, Richert M. Metal forming technology for producing bulk nanostructured metals. Steel Grips. 2004;2:35-44.

[9] Tsuji N, Saito Y, Lee SH, Minamino Y. ARB (accumulative roll-bonding) and other new techniques to produce bulk ultrafine grained materials. Advanced Engineering Materials. 2003;5:338-44.

[10] Valiev RZ, Langdon TG. Principles of equal-channel angular pressing as a processing tool for grain refinement. Progress in Materials Science. 2006;51:881-981.

[11] Valiev RZ, Estrin Y, Horita Z, Langdon TG, Zehetbauer MJ, Zhu YT. Producing bulk ultrafine-grained materials by severe plastic deformation. JOM. 2006;58:33-9.

[12] Huang JY, Zhu YT, Jiang H, Lowe TC. Microstructures and dislocation configurations in nanostructured Cu processed by repetitive corrugation and straightening. Acta Materialia. 2001;49:1497-505.

[13] Tsuji N. Ultrafine grained steels. Tetsu-To-Hagane/Journal of the Iron and Steel Institute of Japan. 2002;88:359-69.

[14] Tsuji N. Formation of Ultrafine Grain of Structure Metals by Severe Plastic Deformation. J Jpn Weld Soc. 2005;74:92.

[15] Nakamura K, Neishi K, Kaneko K, Nakagaki M, Horita Z. Development of severe torsion straining process for rapid continuous grain refinement. Materials Transactions. 2004;45:3338-42.

[16] Valiev RZ, Krasilnikov NA, Tsenev NK. Plastic deformation of alloys with submicron-grained structure. Materials Science and Engineering A. 1991;137:35-40.

[17] Khodabakhshi F, Abbaszadeh M, Eskandari H, Mohebpour SR. Application of CGP-cross route process for microstructure refinement and mechanical properties improvement in steel sheets. Journal of Manufacturing Processes. 2013;15:533-41.

[18] Richert M, Liu Q, Hansen N. Microstructural evolution over a large strain range in aluminium deformed by cyclic-extrusion-compression. Materials Science and Engineering A. 1999;260:275-83.

[19] Mishra RS, Ma ZY. Friction stir welding and processing. Materials Science and Engineering R: Reports. 2005;50:1-78P.

[20] Hirsch J, Skrotzki B, Gottstein G. Aluminium Alloys: The Physical and Mechanical Properties: John Wiley & Sons; 2008.

[21] Chawla KK, Meyers M. Mechanical behavior of materials: Prentice Hall Upper Saddle River; 1999.

[22] Davis JR. Alloying: understanding the basics: ASM international; 2001.

[23] Kaufman JG, Rooy EL. Aluminum alloy castings: properties, processes, and applications: Asm International; 2004.

[24] Wang SC, Starink MJ. Precipitates and intermetallic phases in precipitation hardening Al–Cu–Mg–(Li) based alloys. International Materials Reviews. 2005;50:193-215.

[25] Botelho EC, Silva RA, Pardini LC, Rezende MC. A review on the development and properties of continuous fiber/epoxy/aluminum hybrid composites for aircraft structures. Materials Research. 2006;9:247-56.

[26] Avedesian MM, Baker H. ASM specialty handbook: magnesium and magnesium alloys: ASM international; 1999.

[27] Davis JR, Allen P, Lampman S, Zorc TB, Henry SD, Daquila JL, et al. Metals handbook: properties and selection: nonferrous alloys and special-purpose materials: ASM International; 1990.

[28] Polmear I. Magnesium alloys and applications. Materials science and technology. 1994;10:1-16.

[29] Clark JB. Age hardening in a Mg-9 wt.% Al alloy. Acta Metallurgica. 1968;16:141-52.

[30] Polmear IJ. Magnesium alloys and applications. Materials Science and Technology. 1994;10:1-16.

[31] Horst E, Mordike B. Magnesium technology. metallurgy, design data, application. Springer-Verlag, Berlin Heidelberg; 2006.

[32] Zarandi F, Seale G, Verma R, Essadiqi E, Yue S. Effect of Al and Mn additions on rolling and deformation behavior of AZ series magnesium alloys. Materials Science and Engineering: A. 2008;496:159-68.

[33] Darras BM, Khraisheh MK, Abu-Farha FK, Omar MA. Friction stir processing of commercial AZ31 magnesium alloy. Journal of Materials Processing Technology. 2007;191:77-81.

[34] Abu-Farha F, Khraisheh M. Deformation characteristics of AZ31 magnesium alloy under various forming temperatures and strain rates. Proceedings of the Eighth ESAFORM Conference on Material Forming, Cluj-Napoca, Romania2005. p. 627-30.

[35] Tsao L, Chuang T, Wu C. Evaluation of superplastic formability of the AZ31 magnesium alloy. Zeitschrift für Metallkunde. 2001;92:572-7.

[36] Koike J, Ohyama R, Kobayashi T, Suzuki M, Maruyama K. Grain-boundary sliding in AZ31 magnesium alloys at room temperature to 523 K. Materials Transactions. 2003;44:445-51.

[37] Koike J. Enhanced deformation mechanisms by anisotropic plasticity in polycrystalline Mg alloys at room temperature. Metallurgical and Materials Transactions A. 2005;36:1689-96.

[38] Dieter GE, Bacon DJ. Mechanical metallurgy: McGraw-hill New York; 1986.

[39] Zhao F, Wang L, Fan D, Bie B, Zhou X, Suo T, et al. Macrodeformation twins in single-crystal aluminum. Physical review letters. 2016;116:075501.

[40] Srivatsan TS, Ibrahim I, Mohamed F, Lavernia EJ. Processing techniques for particulate-reinforced metal aluminium matrix composites. Journal of Materials Science. 1991;26:5965-78.

[41] Nardone V, Prewo K. On the strength of discontinuous silicon carbide reinforced aluminum composites. Scripta Metallurgica. 1986;20:43-8.

[42] Lee J, Subramanian K. Failure behaviour of particulate-reinforced aluminium alloy composites under uniaxial tension. Journal of materials science. 1992;27:5453-62.

[43] Ibrahim I, Mohamed F, Lavernia E. Particulate reinforced metal matrix composites—a review. Journal of materials science. 1991;26:1137-56.

[44] Divecha A, Fishman S. Mechanical properties of silicon carbide reinforced aluminum. Mechanical behaviour of materials. 1980:351-61.

[45] Lindroos VK, Talvitie MJ. Recent advances in metal matrix composites. Journal of Materials Processing Technology. 1995;53:273-84.

[46] Erich DL. METAL-MATRIX COMPOSITES: PROBLEMS, APPLICATIONS, AND POTENTIAL IN THE P/M INDUSTRY. Progress in Powder Metallurgy1986. p. 45-65.

[47] Cavaliere P. Mechanical properties of Friction Stir Processed 2618/Al2O3/20p metal matrix composite. Composites Part A: Applied Science and Manufacturing. 2005;36:1657-65.

[48] Bansal NP. Handbook of ceramic composites: Springer Science & Business Media; 2006.

[49] Wahab M, Daud AR, Ghazali MJ. Preparation and characterization of stir cast-aluminum nitride reinforced aluminum metal matrix composites. International Journal of Mechanical and Materials Engineering. 2009;4:115-7.

[50] Reddy AC. Evaluation of Debonding and Dislocation Occurrences in Rhombus Silicon Nitride Particulate/AA4015 Alloy Metal Matrix Composites. 1st National Conference on Modern Materials and Manufacturing, Pune, India1997. p. 278-82.

[51] Chawla N, Shen YL. Mechanical behavior of particle reinforced metal matrix composites. Advanced engineering materials. 2001;3:357-70.

[52] Singla M, Dwivedi DD, Singh L, Chawla V. Development of aluminium based silicon carbide particulate metal matrix composite. Journal of Minerals and Materials Characterization and Engineering. 2009;8:455.

[53] Lou D, Hellman J, Luhulima D, Liimatainen J, Lindroos V. Interactions between tungsten carbide (WC) particulates and metal matrix in WC-reinforced composites. Materials Science and Engineering: A. 2003;340:155-62.

[54] Bourithis L, Milonas A, Papadimitriou G. Plasma transferred arc surface alloying of a construction steel to produce a metal matrix composite tool steel with TiC as reinforcing particles. Surface and Coatings Technology. 2003;165:286-95.

[55] Wu S, Wang H, Tjong S. Mechanical and wear behavior of an Al/Si alloy metal-matrix composite reinforced with aluminosilicate fiber. Composites science and technology. 1996;56:1261-70.

[56] Bakshi SR, Lahiri D, Agarwal A. Carbon nanotube reinforced metal matrix composites-a review. International Materials Reviews. 2010;55:41-64.

[57] Miracle DB. Metal matrix composites - From science to technological significance. Composites Science and Technology. 2005;65:2526-40.

[58] Choo S-H, Lee S, Kwon S-J. Effect of flux addition on the microstructure and hardness of TiC-reinforced ferrous surface composite layers fabricated by high-energy electron beam irradiation. Metallurgical and Materials Transactions A. 1999;30:3131-41.

[59] Choo S-H, Lee S, Kwon S-J. Surface hardening of a gray cast iron used for a diesel engine cylinder block using high-energy electron beam irradiation. Metallurgical and Materials Transactions A. 1999;30:1211-21.

[60] Gui M, Kang SB. 6061Al/Al–SiCp bi-layer composites produced by plasma-spraying process. Materials Letters. 2000;46:296-302.

[61] Hu C, Xin H, Baker TN. Laser processing of an aluminium AA6061 alloy involving injection of SiC particulate. Journal of Materials Science. 1995;30:5985-90.

[62] Lei TC, Ouyang JH, Pei YT, Zhou Y. Microstructure and wear resistance of laser clad TiC particle reinforced coating. Materials Science and Technology. 1995;11:520-5.

[63] Wang Y, Zhang X, Zeng G, Li F. In situ production of Fe-VC and Fe-TiC surface composites by cast-sintering. Composites Part A: Applied Science and Manufacturing. 2001;32:281-6.

[64] Shafiei-Zarghani A, Kashani-Bozorg S, Zarei-Hanzaki A. Microstructures and mechanical properties of Al/Al2O3 surface nano-composite layer produced by friction stir processing. Materials Science and Engineering: A. 2009;500:84-91.

[65] Hosseinzadeh A, Yapici GG. High temperature characteristics of Al2024/SiC metal matrix composite fabricated by friction stir processing. Materials Science and Engineering: A. 2018;731:487-94.

[66] Mishra RS, Mahoney MW, McFadden SX, Mara NA, Mukherjee AK. Scripta Mater. 2000:163-8.

[67] Mishra RS, Mahoney MW. Superplasticity in Advanced Materials, ICSAM'00. 2001;3-357:507-12.

[68] Mishra RS, De PS, Kumar N. Friction Stir Processing. In: Mishra RS, De PS, Kumar N, editors. Friction Stir Welding and Processing: Science and Engineering. Cham: Springer International Publishing; 2014. p. 259-96.

[69] Thomas W, Nicholas E, Needham J, Murch M, Templesmith P, Dawes C. GB Patent application no. 9125978.8, December 1991. Google Scholar. 1995.

[70] Salahi S, Rezazadeh V, Sharbatzadeh A, Iranizad A, Bouzary H. Microstructural refinement of pure copper by friction stir processing. Advanced Materials Research2013. p. 256-61.

[71] Biglari H, Salahi S, Gharajeh SN, Azar MG. Investigation of annealing heat treatment effect on the microstructure and mechanical properties of friction stir welded C70600 copper nickel alloy joints. J Mechatron. 2014;2:119-23.

[72] Lee WB, Lee CY, Chang WS, Yeon YM, Jung SB. Microstructural investigation of friction stir welded pure titanium. Materials Letters. 2005;59:3315-8.

[73] Saito N, Shigematsu I, Komaya T, Tamaki T, Yamauchi G, Nakamura M. Grain refinement of 1050 aluminum alloy by friction stir processing. Journal of materials science letters. 2001;20:1913-5.

[74] Ma Z, Pilchak A, Juhas M, Williams J. Microstructural refinement and property enhancement of cast light alloys via friction stir processing. Scripta Materialia. 2008;58:361-6.

[75] Chang CI, Du XH, Huang JC. Achieving ultrafine grain size in Mg–Al–Zn alloy by friction stir processing. Scripta Materialia. 2007;57:209-12.

[76] Thompson B, Doherty K, Su J, Mishra R. Nano-Sized Grain Refinement Using Friction Stir Processing. In: Mishra R, Mahoney MW, Sato Y, Hovanski Y, Verma R, editors. Friction Stir Welding and Processing VII. Cham: Springer International Publishing; 2016. p. 9-19.

[77] Feng AH, Ma ZY. Enhanced mechanical properties of Mg-Al-Zn cast alloy via friction stir processing. Scripta Materialia. 2007;56:397-400.

[78] Ma ZY, Pilchak AL, Juhas MC, Williams JC. Microstructural refinement and property enhancement of cast light alloys via friction stir processing. Scripta Materialia. 2008;58:361-6.

[79] Liu ZY, Xiao BL, Wang WG, Ma ZY. Singly dispersed carbon nanotube/aluminum composites fabricated by powder metallurgy combined with friction stir processing. Carbon. 2012;50:1843-52.

[80] Izadi H. Fabrication of Metal Matrix Composites by Friction Stir Processing: University of Alberta; 2014.

[81] Sahraeinejad S, Izadi H, Haghshenas M, Gerlich AP. Fabrication of metal matrix composites by friction stir processing with different Particles and processing parameters. Materials Science and Engineering A. 2015;626:505-13.

[82] Bauri R, Yadav D, Suhas G. Effect of friction stir processing (FSP) on microstructure and properties of Al-TiC in situ composite. Materials Science and Engineering A. 2011;528:4732-9.

[83] Mishra RS, Ma ZY. Friction stir welding and processing. Materials Science and Engineering: R: Reports. 2005;50:1-78.

[84] Wang W, Shi Q-y, Liu P, Li H-k, Li T. A novel way to produce bulk SiCp reinforced aluminum metal matrix composites by friction stir processing. Journal of materials processing technology. 2009;209:2099-103.

[85] Su J-Q, Nelson TW, Sterling CJ. A new route to bulk nanocrystalline materials. Journal of materials research. 2003;18:1757-60.

[86] Ma ZY, Sharma SR, Mishra RS. Effect of friction stir processing on the microstructure of cast A356 aluminum. Materials Science and Engineering: A. 2006;433:269-78.

[87] Darras B, Kishta E. Submerged friction stir processing of AZ31 Magnesium alloy. Materials & Design. 2013;47:133-7.

[88] Mishra RS, Ma ZY, Charit I. Friction stir processing: a novel technique for fabrication of surface composite. Materials Science and Engineering: A. 2003;341:307-10.

[89] Alidokht SA, Abdollah-zadeh A, Soleymani S, Assadi H. Microstructure and tribological performance of an aluminium alloy based hybrid composite produced by friction stir processing. Materials & Design. 2011;32:2727-33.

[90] Morisada Y, Fujii H, Nagaoka T, Nogi K, Fukusumi M. Fullerene/A5083 composites fabricated by material flow during friction stir processing. Composites Part A: Applied Science and Manufacturing. 2007;38:2097-101.

[91] Aruri D, Adepu K, Adepu K, Bazavada K. Wear and mechanical properties of 6061-T6 aluminum alloy surface hybrid composites [(SiC+Gr) and (SiC+Al2O3)] fabricated by friction stir processing. Journal of Materials Research and Technology. 2013;2:362-9.

[92] Dolatkhah A, Golbabaei P, Givi MB, Molaiekiya F. Investigating effects of process parameters on microstructural and mechanical properties of Al5052/SiC metal matrix composite fabricated via friction stir processing. Materials & Design. 2012;37:458-64.

[93] Balakrishnan M, Dinaharan I, Palanivel R, Sivaprakasam R. Synthesize of AZ31/TiC magnesium matrix composites using friction stir processing. Journal of Magnesium and Alloys. 2015;3:76-8.

[94] Das S, Mishra R, Doherty K, Cho K, Davis B, DeLorme R. Magnesium Based Composite via Friction Stir Processing. Friction Stir Welding and Processing VII: Springer; 2013. p. 245-52.

[95] Morisada Y, Fujii H, Nagaoka T, Fukusumi M. MWCNTs/AZ31 surface composites fabricated by friction stir processing. Materials science and engineering: A. 2006;419:344-8.

[96] Azizieh M, Kokabi A, Abachi P. Effect of rotational speed and probe profile on microstructure and hardness of AZ31/Al2O3 nanocomposites fabricated by friction stir processing. Materials & Design. 2011;32:2034-41.

[97] Lim C, Lim S, Gupta M. Wear behaviour of SiCp-reinforced magnesium matrix composites. Wear. 2003;255:629-37.

[98] Lee CJ, Huang JC, Hsieh PJ. Mg based nano-composites fabricated by friction stir processing. Scripta Materialia. 2006;54:1415-20.

[99] Don-Hyun C, Yong-Il K, Dae-Up K, Seung-Boo J. Effect of SiC particles on microstructure and mechanical property of friction stir processed AA6061-T4. Transactions of Nonferrous Metals Society of China. 2012;22:s614-s8.

[100] Mahmoud E, Takahashi M, Shibayanagi T, Ikeuchi K. Effect of friction stir processing tool probe on fabrication of SiC particle reinforced composite on aluminium surface. Science and Technology of Welding and Joining. 2009;14:413-25.

[101] Asadi P, Faraji G, Besharati MK. Producing of AZ91/SiC composite by friction stir processing (FSP). The International Journal of Advanced Manufacturing Technology. 2010;51:247-60.

[102] Koilraj M, Sundareswaran V, Vijayan S, Rao SK. Friction stir welding of dissimilar aluminum alloys AA2219 to AA5083–Optimization of process parameters using Taguchi technique. Materials & Design. 2012;42:1-7.

[103] Lakshminarayanan A, Balasubramanian V. Process parameters optimization for friction stir welding of RDE-40 aluminium alloy using Taguchi technique. Transactions of Nonferrous Metals Society of China. 2008;18:548-54.

[104] Liu H, Maeda M, Fujii H, Nogi K. Tensile properties and fracture locations of friction-stir welded joints of 1050-H24 aluminum alloy. Journal of Materials Science Letters. 2003;22:41-3.

[105] Hassan KAA, Prangnell PB, Norman AF, Price DA, Williams SW. Effect of welding parameters on nugget zone microstructure and properties in high strength aluminium alloy friction stir welds. Science and Technology of Welding and Joining. 2003;8:257-68.

[106] Park SHC, Sato YS, Kokawa H. Microstructural evolution and its effect on Hall-Petch relationship in friction stir welding of thixomolded Mg alloy AZ91D. Journal of Materials Science. 2003;38:4379-83.

[107] Park HS, Kimura T, Murakami T, Nagano Y, Nakata K, Ushio M. Microstructures and mechanical properties of friction stir welds of 60% Cu–40% Zn copper alloy. Materials Science and Engineering: A. 2004;371:160-9.

[108] Akramifard H, Shamanian M, Sabbaghian M, Esmailzadeh M. Microstructure and mechanical properties of Cu/SiC metal matrix composite fabricated via friction stir processing. Materials & Design (1980-2015). 2014;54:838-44.

[109] Feng A, Ma Z. Microstructural evolution of cast Mg–Al–Zn during friction stir processing and subsequent aging. Acta Materialia. 2009;57:4248-60.

[110] Humphreys FJ, Prangnell PB, Priestner R. Fine-grained alloys by thermomechanical processing. Current Opinion in Solid State and Materials Science. 2001;5:15-21.

[111] Azizieh M, Kokabi AH, Abachi P. Effect of rotational speed and probe profile on microstructure and hardness of AZ31/Al2O3 nanocomposites fabricated by friction stir processing. Materials & Design. 2011;32:2034-41.

[112] Peat T, Galloway A, Toumpis A, McNutt P, Iqbal N. The erosion performance of cold spray deposited metal matrix composite coatings with subsequent friction stir processing. Applied Surface Science. 2017;396:1635-48.

[113] Hsu C, Chang C, Kao P, Ho N, Chang C. Al–Al 3 Ti nanocomposites produced in situ by friction stir processing. Acta Materialia. 2006;54:5241-9.

[114] Liu Q, Ke L, Liu F, Huang C, Xing L. Microstructure and mechanical property of multi-walled carbon nanotubes reinforced aluminum matrix composites fabricated by friction stir processing. Materials & Design. 2013;45:343-8.

[115] Shafiei-Zarghani A, Kashani-Bozorg S, Zarei-Hanzaki A. Microstructures and mechanical properties of Al/Al 2 O 3 surface nano-composite layer produced by friction stir processing. Materials Science and Engineering: A. 2009;500:84-91.

[116] Tjong SC. Novel nanoparticle-reinforced metal matrix composites with enhanced mechanical properties. Advanced engineering materials. 2007;9:639-52.

[117] Picu RC, Vincze G, Ozturk F, Gracio JJ, Barlat F, Maniatty AM. Strain rate sensitivity of the commercial aluminum alloy AA5182-O. Materials Science and Engineering: A. 2005;390:334-43.

[118] Shojaei K, Sajadifar SV, Yapici GG. On the mechanical behavior of cold deformed aluminum 7075 alloy at elevated temperatures. Materials Science and Engineering: A. 2016;670:81-9.

[119] Takai R, Kimura S, Kashiuchi R, Kotaki H, Yoshida M. Grain refinement effects on the strain rate sensitivity and grain boundary sliding in partially solidified Al–5wt%Mg alloy. Materials Science and Engineering: A. 2016;667:417-25.

[120] Kreitcberg A, Brailovski V, Prokoshkin S, Gunderov D, Khomutov M, Inaekyan K. Effect of the grain/subgrain size on the strain-rate sensitivity and deformability of Ti–50at%Ni alloy. Materials Science and Engineering: A. 2015;622:21-9.

[121] Zhou M, Lin Y, Deng J, Jiang Y-Q. Hot tensile deformation behaviors and constitutive model of an Al–Zn–Mg–Cu alloy. Materials & Design. 2014;59:141-50.

[122] Sajadifar SV, Yapici GG. Workability characteristics and mechanical behavior modeling of severely deformed pure titanium at high temperatures. Materials & Design. 2014;53:749-57.

[123] Halim H, Wilkinson DS, Niewczas M. The Portevin–Le Chatelier (PLC) effect and shear band formation in an AA5754 alloy. Acta Materialia. 2007;55:4151-60.

[124] Chatterjee A, Murty K, Gayathri N, Mukherjee P, Barat P. Temperature dependence of the dynamics of portevin-le chatelier effect in al-2.5 pct mg alloy. Metallurgical and Materials Transactions A. 2011;42:1184-90.

[125] Charnock W. The influence of grain size on the nature of portevin-lechatelier yielding. The Philosophical Magazine: A Journal of Theoretical Experimental and Applied Physics. 1968;18:89-99.

[126] Park K-T, Hwang D-Y, Lee Y-K, Kim Y-K, Shin DH. High strain rate superplasticity of submicrometer grained 5083 Al alloy containing scandium fabricated by severe plastic deformation. Materials science and engineering: A. 2003;341:273-81.

[127] Cavaliere P. Mechanical properties of friction stir processed 2618/Al 2 O 3/20p metal matrix composite. Composites Part A: applied science and manufacturing. 2005;36:1657-65.

[128] LU J, JIN L, DONG J, ZENG X-q, DING W-j, YAO Z-y. Deformation behaviors of AZ31 magnesium alloy by equal channel angular extrusion [J]. The Chinese Journal of Nonferrous Metals. 2009;3:007.

[129] Lin Y, Deng J, Jiang Y-Q, Wen D-X, Liu G. Hot tensile deformation behaviors and fracture characteristics of a typical Ni-based superalloy. Materials & Design. 2014;55:949-57.

[130] Chinh NQ, Csanádi T, Gubicza J, Valiev R, Straumal B, Langdon TG. The effect of grain boundary sliding and strain rate sensitivity on the ductility of ultrafine-grained materials. Materials Science Forum: Trans Tech Publ; 2011. p. 677-82.

[131] Samei J, Zhou L, Kang J, Wilkinson DS. Microstructural analysis of ductility and fracture in fine-grained and ultrafine-grained vanadium-added DP1300 steels. International Journal of Plasticity. 2018.

[132] Pineau A, Benzerga AA, Pardoen T. Failure of metals I: Brittle and ductile fracture. Acta Materialia. 2016;107:424-83.

[133] Yuvaraj N, Aravindan S, Vipin. Fabrication of Al5083/B4C surface composite by friction stir processing and its tribological characterization. Journal of Materials Research and Technology. 2015;4:398-410.

[134] Lim DK, Shibayanagi T, Gerlich AP. Synthesis of multi-walled CNT reinforced aluminium alloy composite via friction stir processing. Materials Science and Engineering: A. 2009;507:194-9.

[135] Svensson LE, Karlsson L, Larsson H, Karlsson B, Fazzini M, Karlsson J. Microstructure and mechanical properties of friction stir welded aluminium alloys with special reference to AA 5083 and AA 6082. Science and Technology of Welding and Joining. 2000;5:285-96.

[136] Chen CM, Kovacevic R. Finite element modeling of friction stir welding—thermal and thermomechanical analysis. International Journal of Machine Tools and Manufacture. 2003;43:1319-26.

[137] Benavides S, Li Y, Murr LE, Brown D, McClure JC. Low-temperature friction-stir welding of 2024 aluminum. Scripta Materialia. 1999;41:809-15.

[138] Ceschini L, Minak G, Morri A. Tensile and fatigue properties of the AA6061/20vol% Al2O3p and AA7005/10vol% Al2O3p composites. Composites Science and Technology. 2006;66:333-42.

[139] Zhao D, Tuler FR, Lloyd DJ. Fracture at elevated temperatures in a particle reinforced composite. Acta Metallurgica et Materialia. 1994;42:2525-33.

[140] Chang CI, Lee CJ, Huang JC. Relationship between grain size and Zener–Holloman parameter during friction stir processing in AZ31 Mg alloys. Scripta Materialia. 2004;51:509-14.

[141] Mukai T, Yamanoi M, Higashi K. Processing of Ductile Magnesium Alloy under Dynamic Tensile Loading. Materials Transactions. 2001;42:2652-4.

[142] Kim WJ, Hong SI, Kim YS, Min SH, Jeong HT, Lee JD. Texture development and its effect on mechanical properties of an AZ61 Mg alloy fabricated by equal channel angular pressing. Acta Materialia. 2003;51:3293-307.

[143] Kim WJ, Jeong HT. Grain-Size Strengthening in Equal-Channel-Angular-Pressing Processed AZ31 Mg Alloys with a Constant Texture. Materials Transactions. 2005;46:251-8.

[144] Peel M, Steuwer A, Preuss M, Withers PJ. Microstructure, mechanical properties and residual stresses as a function of welding speed in aluminium AA5083 friction stir welds. Acta Materialia. 2003;51:4791-801.

[145] Charit I, Mishra RS. High strain rate superplasticity in a commercial 2024 Al alloy via friction stir processing. Materials Science and Engineering: A. 2003;359:290-6.

[146] Sato Y, Park S, Matsunaga A, Honda A, Kokawa H. Novel production for highly formable Mg alloy plate. Journal of Materials Science. 2005;40:637-42.

[147] Rokni M, Zarei-Hanzaki A, Roostaei AA, Abedi H. An investigation into the hot deformation characteristics of 7075 aluminum alloy. Materials & Design. 2011;32:2339-44.

[148] Doherty R, Hughes D, Humphreys F, Jonas J, Jensen DJ, Kassner M, et al. Current issues in recrystallization: a review. Materials Science and Engineering: A. 1997;238:219-74.

VITA

Ali Hosseinzadeh Ghobadlou was born in 1990 in Tehran. He received his B.Sc. in Mechanical Engineering from University of Tabriz, Iran in 2013 and he is currently pursuing the M.Sc. degree in Mechanical Engineering at Ozyegin University. His research interests at MEMFIS group of Ozyegin University mainly concentrates on the mechanical properties of light alloys and metal matrix composites processed by severe plastic deformation.